Euro. Jnl of Applied Mathematics (2015), *vol.* 26, *pp.* 743–772.
doi:10.1017/S0956792515000327

Straining flow of a weakly interacting polymer–surfactant solution

C. J. W. BREWARD, I. M. GRIFFITHS, P. D. HOWELL and C. E. MORGAN

Mathematical Institute, University of Oxford, Oxford OX2 6GG, UK
email: breward@maths.ox.ac.uk; ian.griffiths@maths.ox.ac.uk; howell@maths.ox.ac.uk; cara.e.morgan@gmail.com

(*Received 6 January 2015; revised 11 June 2015; accepted 11 June 2015; first published online 16 July 2015*)

In this paper, we consider the straining flow of a weakly interacting polymer–surfactant solution below a free surface, with the bulk surfactant concentration above the critical micelle concentration. We formulate a set of coupled differential equations describing the concentration of monomers, micelles, polymer, and polymer–micelle aggregates in the flow. We analyse the model in several asymptotic limits, and make predictions about the distribution of each of the species. In particular, in the large-reaction-rate limit we find that the model predicts a region near the free surface where no micelles or aggregates are present, and beneath this a region where the concentration of surfactant is constant, across which the concentration of aggregates increases until all the free polymer is consumed. For certain parameter regimes, a maximum in the concentration of the polymer–micelle complex occurs within the bulk fluid. In the finite-reaction-rate limit, micelles, and aggregates are present right up to the free surface, and the plateau in the concentration of surfactant in the bulk is no longer present. Results from the asymptotic theory compare favorably with full numerical solutions.

Key words: Surfactants; boundary layers; asymptotic analysis; advection-diffusion-reaction equations

1 Introduction

Surfactants are widely used in industry where they reduce surface tension, enhance spreading, and enable cleansing. Surfactants are amphiphilic molecules containing both oil-soluble and water-soluble components. Near air–liquid interfaces, it is energetically favourable for them to adsorb at the interface, expel their oil-soluble tails and, in doing so, reduce the surface tension. At sufficiently high concentrations, it is also possible for surfactants to shield their oil-soluble tails from water by forming aggregates called micelles, which are often spherical for moderate surfactant concentrations. The concentration of surfactant at which these micelles start to form is known as the Critical Micelle Concentration (CMC).

Polymers are often added to surfactant solutions [17] to control the rheology and stability of the system, for example, in fabric and hair conditioners. The presence of neutral or charged polymers in an aqueous solution of ionic surfactant causes a marked change in the surface tension profile [2]. In the case where the polymer is neutral, the interactions

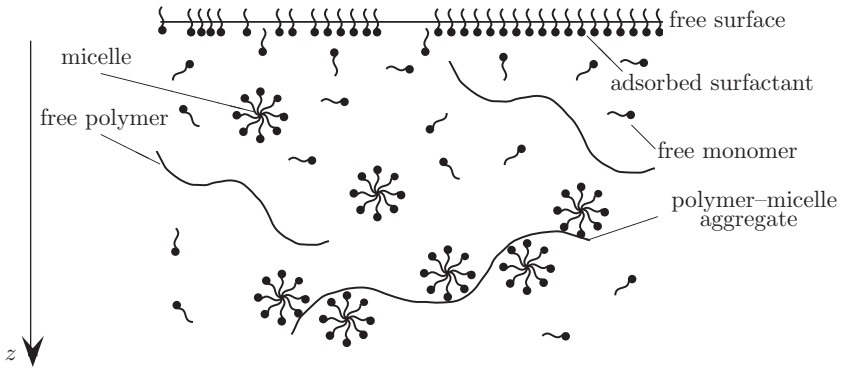

FIGURE 1. Schematic diagram of a weakly interacting polymer-surfactant system.

between polymer and surfactant are mainly driven by weak hydrophobic forces and the system is called "weakly interacting" [5]. In the case where the polymer is charged, the interactions are mainly driven by electrostatic forces and the system is called "strongly interacting" [6]. We focus our attention in this paper on weakly interacting systems, as shown in the schematic in Figure 1. In these systems, surfactant molecules adsorb at any air-liquid interfaces but if the concentration is increased it is also energetically favourable for the surfactant monomers to form complexes with the polymers in the bulk. These complexes comprise single polymer chains with small micelles attached to them, and they are commonly known as polymer–micelle aggregates. The number of monomers that form the micelles incorporated into a polymer–micelle aggregate is normally lower than the number of monomers that make up a "free" micelle. The surfactant concentration at which the aggregates start to form in the bulk is known as the Critical Aggregation Concentration (CAC) [5], and this is usually below the CMC.

A comprehensive summary of the experimental and theoretical work on polymer–surfactant mixtures is presented in the articles by Goddard [10–12] and the books [13,15]. Recent studies have focused on explaining the effects of polymer–surfactant systems on interfacial tension [2] as well as the improved stability offered by such mixtures over copolymers in the resulting foam structures that form at interfaces [16].

The overflowing cylinder experiment (see Bain [4]) provides a controlled environment for studying the dynamic surface properties of surfactant solutions in a non-invasive way. In the experiment, water is pumped up the inside of a cylinder, forms a flat free surface and flows over the rim of the cylinder and down the outside, where it is collected and recirculated. Liquid at the free surface flows radially outwards from a stagnation point at the centre (see Breward *et al.* [7], Howell and Breward [14]). The cylinder is carefully levelled so that it overflows uniformly on all sides and once a stable flow has been established the free surface away from the rim is indistinguishable from a horizontal plane.

We use this set-up to motivate our current study, and it builds on previous work on shearing flow of surfactant-only systems as described in Breward and Howell [8]. Breward and Howell [8] consider a surfactant solution which is above the CMC far away from a free surface, and assume that a monolayer of surfactant adsorbs at the free surface.

https://doi.org/10.1017/S0956792515000327 Published online by Cambridge University Press

Since the free surface is expanding, the concentration of adsorbed surfactant decreases and must be replenished from the bulk. They found that the subsequent decrease in bulk surfactant concentration locally near the free surface results in micelle dissociation, and matched the model with experimental data to determine whether or not the reaction between monomer and micelles was in equilibrium.

In this paper, we will extend the results in [8] to include polymer and polymer–micelle aggregates. In Section 2, we will formulate our model, while in Section 3, we will consider the asymptotic limit in which the reaction rates are large. In Section 4, we will consider the case of finite reaction rates. Finally, in Section 5, we will draw conclusions. We are unaware of any existing experimental results on the shearing flow of polymer–surfactant solutions; we hope the development of this theory will stimulate future experiments and enable validation.

2 Model

We consider the flow of an aqueous polymer–surfactant solution above the CMC (and hence also above the CAC). We denote the concentrations of surfactant monomers, micelles, polymers, and polymer–micelle aggregates by S, S_m, P, and P_m respectively, each measured in mol m^{-3}. We follow [8] and assume that the reactions forming micelles and aggregates are single-step reactions, and invoking the law of mass action we find that the rate, j_0, at which surfactant changes phase from monomer to micelle is given by

$$j_0 = k_0^+ S^N - k_0^- S_m, \tag{2.1}$$

where $k_0^\pm$ are the corresponding rate coefficients and N is the number of surfactant monomers in a free micelle. Similarly the rate, j_1, at which surfactant monomers combine with polymers to form aggregates is given by

$$j_1 = k_1^+ P S^M - k_1^- P_m, \tag{2.2}$$

where $k_1^\pm$ are the corresponding rate coefficients and $M = nm$ where n is the number of surfactant monomers in a polymer-bound micelle and m is the number of micelles in a polymer–micelle aggregate. We refer to N and M as the aggregation numbers for a micelle and a polymer–micelle aggregate respectively. Typical values for the aggregation numbers are $N \sim 80$ and $M \sim 200$ [9,18].

We suppose that z is the distance into the fluid measured from the free surface and that r is the radial distance from the centre of the cylinder. If all phases are advected with fluid velocity $\mathbf{u}$ while also diffusing, after an initial set-up phase the four concentrations satisfy the steady reaction-advection-diffusion equations

$$\mathbf{u}\cdot\nabla S = D_S\nabla^2 S - N j_0 - M j_1, \qquad \mathbf{u}\cdot\nabla S_m = D_{S_m}\nabla^2 S_m + j_0, \tag{2.3a}$$

$$\mathbf{u}\cdot\nabla P = D_P\nabla^2 P - j_1, \qquad \mathbf{u}\cdot\nabla P_m = D_{P_m}\nabla^2 P_m + j_1, \tag{2.3b}$$

where D_S, D_{S_m}, D_P, and D_{P_m} are the diffusion coefficients for each phase. At the free surface, located at $z = 0$, we assume that only surfactant monomers can adsorb and denote the concentration of adsorbed surfactant molecules by Γ. If we neglect surface

https://doi.org/10.1017/S0956792515000327 Published online by Cambridge University Press

diffusion (for justification, see [7]) then Γ evolves through advection along the interface, with surface velocity $\mathbf{u}_s(r) = \mathbf{u}(r, 0)$, and replenishment by monomer from the bulk and it satisfies, after the initial set up phase,

$$D_S \frac{\partial S}{\partial z} = \nabla \cdot (\mathbf{u}_s \Gamma) \quad \text{at} \quad z = 0. \tag{2.4}$$

We also assume that the adsorbed phase is in thermodynamic equilibrium with the free surfactant monomers just below the surface so we can use the Langmuir isotherm [1] to determine Γ in terms of S,

$$\Gamma = \frac{\Gamma_{\text{sat}} S}{k + S} \quad \text{at} \quad z = 0, \tag{2.5}$$

where k is a constant measuring the ability of the surfactant monomers to adsorb at the interface and Γ_{sat} is the maximum concentration that the adsorbed surfactant monomers can attain.

In weakly interacting systems, free polymers are not surface active and hence do not adsorb at the interface. Further, micelles and polymer–micelle aggregates do not directly adsorb without first breaking up into monomers. Thus, the fluxes of S_m, P, and P_m must be zero at the interface:

$$D_{S_m} \frac{\partial S_m}{\partial z} = D_P \frac{\partial P}{\partial z} = D_{P_m} \frac{\partial P_m}{\partial z} = 0 \quad \text{at} \quad z = 0. \tag{2.6}$$

Far away from the interface we assume that the surfactant and micelle concentrations are in equilibrium and that the free polymer and aggregate concentrations are in equilibrium, *i.e.*

$$S_m \sim \frac{k_0^+}{k_0^-} S^N, \qquad \text{and} \qquad P_m \sim \frac{k_1^+}{k_1^-} P S^M \qquad \text{as} \quad z \to \infty. \tag{2.7}$$

We also assume that, far away from the interface, the total bulk concentrations of surfactant and polymer, S_b and P_b respectively, are known, so that

$$S + N S_m + M P_m \to S_b, \qquad \text{and} \qquad P + P_m \to P_b \qquad \text{as} \quad z \to \infty. \tag{2.8}$$

In principle, the velocity $\mathbf{u}$ is coupled to the concentration through the surface tension gradient, and the solution to the coupled surfactant-fluid mechanics problem is presented in Howell and Breward [14]. However, near the axis of the overflowing cylinder, there is a stagnation point flow whose strength may be measured experimentally [3]. Therefore, we assume in this paper that the fluid velocity $\mathbf{u}$ is a known function of r and z, given by

$$\mathbf{u} = \frac{\alpha r}{2} \mathbf{e}_r - \alpha z \mathbf{e}_z, \tag{2.9}$$

where $\mathbf{e}_r$ and $\mathbf{e}_z$ are the unit vectors in the r and z directions respectively, and α is the strength of the flow. We suppose that α is a known parameter (in principle it is determined by global conditions on the flow, as shown in [14]). Then (2.3)–(2.9) form a closed system of equations for S, S_m, P, and P_m.

https://doi.org/10.1017/S0956792515000327 Published online by Cambridge University Press

2.1 Nondimensionalisation

We nondimensionalise (2.3*a*)–(2.9) using the following scalings:

$$S = S_{\mathrm{CMC}}\bar{S}, \qquad S_m = \frac{S_{\mathrm{CMC}}}{N}\bar{S}_m, \qquad P = P_b\bar{P}, \qquad P_m = P_b\bar{P}_m,$$
$$\Gamma = \Gamma_{\mathrm{sat}}\bar{\Gamma}, \qquad \mathbf{u} = \sqrt{\alpha D_S}\bar{\mathbf{u}}, \qquad r = \sqrt{\frac{D_s}{\alpha}}\bar{r}, \qquad z = \sqrt{\frac{D_s}{\alpha}}\bar{z}, \tag{2.10}$$

where S_{CMC} is the CMC for the surfactant. We define the CMC and the CAC for the surfactant as in Bell *et al.* [5] by the expressions,

$$S_{\mathrm{CMC}} = \left(\frac{k_0^-}{Nk_0^+}\right)^{\frac{1}{N-1}} \quad \text{and} \quad S_{\mathrm{CAC}} = \left(\frac{k_1^-}{k_1^+}\right)^{\frac{1}{M}}, \tag{2.11}$$

respectively. For ease of notation we drop the bars on the dimensionless variables and the resulting dimensionless system of equations is

$$\mathbf{u}\cdot\nabla S = \nabla^2 S - K_0\left(S^N - S_m\right) - K_1P^*\left(P\left(S/\delta\right)^M - P_m\right), \tag{2.12a}$$
$$\mathbf{u}\cdot\nabla S_m = D_1\nabla^2 S_m + K_0\left(S^N - S_m\right), \tag{2.12b}$$
$$\mathbf{u}\cdot\nabla P = D_2\nabla^2 P - K_1\left(P\left(S/\delta\right)^M - P_m\right), \tag{2.12c}$$
$$\mathbf{u}\cdot\nabla P_m = D_3\nabla^2 P_m + K_1\left(P\left(S/\delta\right)^M - P_m\right), \tag{2.12d}$$

with boundary conditions

$$S_m \to S^N, \quad P_m \to P\left(S/\delta\right)^M, \quad P + P_m \to 1, \quad S + S_m + P^*P_m \to S^*, \quad \text{as} \quad z \to \infty, \tag{2.12e}$$
$$\frac{1}{\Gamma^*}\frac{\partial S}{\partial z} = \nabla\cdot(\mathbf{u}_s\Gamma), \quad \frac{\partial S_m}{\partial z} = \frac{\partial P}{\partial z} = \frac{\partial P_m}{\partial z} = 0, \quad \Gamma = \frac{S}{S+\beta} \quad \text{on} \quad z = 0. \tag{2.12f}$$

The dimensionless parameters of the model are

$$S^* = \frac{S_b}{S_{\mathrm{CMC}}}, \quad P^* = \frac{MP_b}{S_{\mathrm{CMC}}}, \quad \Gamma^* = \frac{\Gamma_{\mathrm{sat}}}{S_{\mathrm{CMC}}}\sqrt{\frac{\alpha}{D_s}}, \quad \delta = \frac{S_{\mathrm{CAC}}}{S_{\mathrm{CMC}}}, \quad \beta = \frac{k}{S_{\mathrm{CMC}}},$$
$$K_0 = \frac{k_0^-}{\alpha}, \quad K_1 = \frac{k_1^-}{\alpha}, \quad D_1 = \frac{D_{S_m}}{D_S}, \quad D_2 = \frac{D_P}{D_S}, \quad D_3 = \frac{D_{P_m}}{D_S}. \tag{2.13}$$

We seek a solution in which the concentrations only depend on z and this reduces the model to:

$$S'' + zS' = K_0\left(S^N - S_m\right) + K_1P^*\left(P\left(S/\delta\right)^M - P_m\right), \tag{2.14a}$$
$$D_1S_m'' + zS_m' = -K_0\left(S^N - S_m\right), \tag{2.14b}$$
$$D_2P'' + zP' = K_1\left(P\left(S/\delta\right)^M - P_m\right), \tag{2.14c}$$
$$D_3P_m'' + zP_m' = -K_1\left(P\left(S/\delta\right)^M - P_m\right), \tag{2.14d}$$

https://doi.org/10.1017/S0956792515000327 Published online by Cambridge University Press

where primes denote differentiation with respect to z. The boundary conditions become

$$S_m \to S^N, \quad P_m \to P\left(S/\delta\right)^M, \quad P+P_m \to 1, \quad S+S_m+P^*P_m \to S^* \quad \text{as} \quad z \to \infty, \tag{2.14e}$$

$$S' = \Gamma^*\Gamma = \frac{\Gamma^* S}{\beta + S} \quad \text{and} \quad P' = S_m' = P_m' = 0 \quad \text{on} \quad z = 0. \tag{2.14f}$$

2.2 Parameter values

The dimensionless parameters N, M, S^*, P^*, δ, β, D_1, D_2, and D_3 depend only on the surfactant and polymer under consideration. Of these, N and M are large, $O(10-200)$, and β is usually small, about $O(10^{-2})$. The CAC is assumed to be less than the CMC but not by more than an order of magnitude so typically $\delta = O(10^{-1})$. We suppose that, in situations of practical interest, the bulk surfactant concentration is a few times the CMC and that P^* is also $O(1)$. The diffusivities of the larger species S_m, P, and P_m are typically less than the diffusivity of the free monomers but not by more than an order of magnitude, so that $D_i = O(10^{-1})$ for $i = 1, 2, 3$.

The parameters Γ^*, K_0, and K_1 all depend on the flow rate α. We assume that Γ^* is $O(1)$, but K_0 and K_1 are proportional to the micelle and polymer–micelle aggregate dissociation rates respectively, which in general are not known. However, these processes are widely believed to be nearly instantaneous in the polymer–surfactant systems we are concerned with, which implies that K_0 and K_1 are large. Thus, in the analysis that follows in the next section, we take the limit $K_0, K_1 \to \infty$ with K_0/K_1 fixed, which corresponds to both the monomer/micellar phases and the polymer/polymer–micelle aggregate phases being in equilibrium everywhere.

3 The large K_0 and K_1 limit

The system given in (2.14) reduces considerably when the reaction rates are much faster than the flow strength. In this limit, K_0 and K_1 are both large (with ratio $K_0/K_1 \sim O(1)$) and so we formally let $K_0, K_1 \to \infty$ with $K_0/K_1 = \kappa$ fixed. We find that the monomer and micellar phases are in equilibrium, as are the polymer and aggregates, so that

$$S_m = S^N, \qquad P_m = P\left(S/\delta\right)^M. \tag{3.1a}$$

We are then able to simplify the model to a system of two coupled ordinary differential equations for the surfactant and polymer concentrations, namely

$$\left(S + D_1 S^N + D_3 P^* P\left(S/\delta\right)^M\right)'' + z\left(S + S^N + P^* P\left(S/\delta\right)^M\right)' = 0, \tag{3.1b}$$

$$\left(D_2 P + D_3 P\left(S/\delta\right)^M\right)'' + z\left(P + P\left(S/\delta\right)^M\right)' = 0, \tag{3.1c}$$

with

$$P + P\left(S/\delta\right)^M \to 1, \qquad S + S^N + P^* P\left(S/\delta\right)^M \to S^* \qquad \text{as} \qquad z \to \infty, \tag{3.1d}$$

https://doi.org/10.1017/S0956792515000327 Published online by Cambridge University Press

$$S' = \frac{\Gamma^* S}{\beta + S} \quad \text{and} \qquad S'_m = P' = P'_m = 0 \qquad \text{on} \quad z = 0. \tag{3.1e}$$

We can immediately see that, with the forms for S_m and P_m given by (3.1*a*), we will not be able to satisfy the corresponding boundary conditions for S_m and P_m in (2.14*f*) and hence we expect there to be a boundary layer at the free surface across which the flux of each species adjusts.

3.1 All diffusivities are the same

We illustrate the structure of the problem in the particularly simple case when all the diffusivities are the same, *i.e.* $D_1 = D_2 = D_3 = 1$. In this case, we can integrate (3.1*b*)–(3.1*c*) directly and use the boundary conditions at infinity to obtain:

$$S + S^N + P^* P \left(S/\delta\right)^M = S^* + a \operatorname{erfc}\left(\frac{z}{\sqrt{2}}\right), \tag{3.2}$$

$$P + P \left(S/\delta\right)^M = 1 + b \operatorname{erfc}\left(\frac{z}{\sqrt{2}}\right), \tag{3.3}$$

where a and b are constants of integration. We rearrange (3.3) and use (3.1*a*) to find that

$$P = \frac{\delta^M}{\delta^M + S^M}\left(1 + b \operatorname{erfc}\left(\frac{z}{\sqrt{2}}\right)\right), \quad P_m = \frac{S^M}{\delta^M + S^M}\left(1 + b \operatorname{erfc}\left(\frac{z}{\sqrt{2}}\right)\right), \tag{3.4}$$

while S and S_m are given by

$$S + S^N + P^* \frac{S^M}{\delta^M + S^M}\left(1 + b \operatorname{erfc}\left(\frac{z}{\sqrt{2}}\right)\right) = S^* + a \operatorname{erfc}\left(\frac{z}{\sqrt{2}}\right), \quad S_m = S^N, \tag{3.5}$$

using (3.1*a*) and (3.2). At $z = 0$,

$$S' = \frac{\sqrt{\frac{2}{\pi}}\left(\frac{P^* S^M}{\delta^M + S^M} b - a\right)}{1 + NS^{N-1} + \frac{P^* M \delta^M S^{M-1}(1+b)}{\left(\delta^M + S^M\right)^2}}, \tag{3.6}$$

$$S'_m = NS^{N-1} S', \tag{3.7}$$

$$P' = -\frac{\delta^M}{\delta^M + S^M}\sqrt{\frac{2}{\pi}} b - \frac{M \delta^M S^{M-1}(1+b)}{(\delta^M + S^M)^2} S', \tag{3.8}$$

$$P'_m = -\frac{S^M}{\delta^M + S^M}\sqrt{\frac{2}{\pi}} b + \frac{M \delta^M S^{M-1}(1+b)}{(\delta^M + S^M)^2} S'. \tag{3.9}$$

As noted earlier, (3.6) and (3.9) cannot satisfy all the boundary conditions at $z = 0$ and thus there is a boundary layer near $z = 0$ in which the reactions are out of equilibrium. We illustrate the boundary layer calculation, in the case where the bulk concentration is such that there are no micelles present, in Appendix A. The boundary layer calculation in other cases follows the same recipe. The boundary layer has the obvious width $O(1/\sqrt{K_1})$ and we find that each of the concentrations is constant across the layer to leading order

https://doi.org/10.1017/S0956792515000327 Published online by Cambridge University Press

in $1/\sqrt{K_1}$. To match with the outer solution we solve the $O(1/\sqrt{K_1})$ equations in the boundary layer, and we find that

$$b = 0, \qquad a = -\sqrt{\frac{\pi}{2}}\frac{\Gamma^* S_i}{\beta + S_i}, \tag{3.10}$$

where S_i is the leading-order (constant) concentration of surfactant in the boundary layer. We thus find that the outer solution is:

$$S_m = S^N, \quad P = \frac{\delta^M}{\delta^M + S^M}, \quad P_m = \frac{S^M}{\delta^M + S^M}, \tag{3.11a}$$

$$S + S^N + P^* \frac{S^M}{\delta^M + S^M} = S^* - \sqrt{\frac{\pi}{2}}\frac{\Gamma^* S_i}{\beta + S_i}\ \mathrm{erfc}\left(\frac{z}{\sqrt{2}}\right), \tag{3.11b}$$

with S_i given by

$$S_i + S_i^N + \frac{P^* S_i^M}{\delta^M + S_i^M} = S^* - \sqrt{\frac{\pi}{2}}\frac{\Gamma^* S_i}{\beta + S_i}. \tag{3.11c}$$

We note that Breward and Howell [8] do not consider the boundary layer and comparison between (3.11c) in the case $P^* = 0$ and equation (3.3) in [8] highlights an erroneous factor of nC_0^n ($C_0 = S_i$, $n = N$ in the notation of [8]). The consequence is that, as the subsurface concentration approaches the CMC, Breward and Howell [8] significantly underpredict the subsurface surfactant concentration and the resulting micellar concentration. For example, Figure 3(b) in [8] should have $S_m(0) \approx 0.76$, rather than $S_m(0) \approx 0$ as shown there.

We show in Figure 2(a) the variation of the subsurface concentration S_i with bulk surfactant concentration S^*, given by (3.11c) for several values of P^*. We see that, as P^* increases, a plateau-like structure forms at around $S_i = \delta$, where the subsurface concentration is nearly constant as S^* is increased. This is to be expected: near the CAC, increasing the bulk concentration increases the concentration of complexes rather than the monomer concentration. In Figure 2(b), we compare the S_i versus S^* graphs given by solving (3.11c) in the two cases $\Gamma^* = 2$ and $\Gamma^* = 0$ (the latter corresponding to the equilibrium case where there is no flow). We see that the flow dramatically reduces the amount of surfactant arriving at the free surface for a given bulk concentration. The effect is especially pronounced for bulk concentrations up to $S^* \sim 1 + P^* + \Gamma^*\sqrt{\pi/2}$.

In Figure 3 we show how the concentrations vary with depth for various values of the bulk surfactant concentration S^*. On first glance, these concentration profiles appear to be non-smooth. However, these plots are well resolved and smooth and the apparent sharp corners are simply a result of the large values of M and N. In Figure 3(a), we illustrate the case where the bulk surfactant concentration is above the CAC but below the CMC, and in which the flow causes the surface concentration to be below the CAC. Close to the free surface, the surfactant concentration is below the CAC, there are no complexes and all the polymer is free. The monomer concentration increases with depth until it reaches the CAC and then plateaus. Below this depth, complexes start to form and the free polymer becomes depleted. Far away from the free surface, polymer and complex coexist, and the monomer concentration is constant (and at the CAC). As we increase the bulk concentration to be above the CMC, we arrive in a situation where the

https://doi.org/10.1017/S0956792515000327 Published online by Cambridge University Press

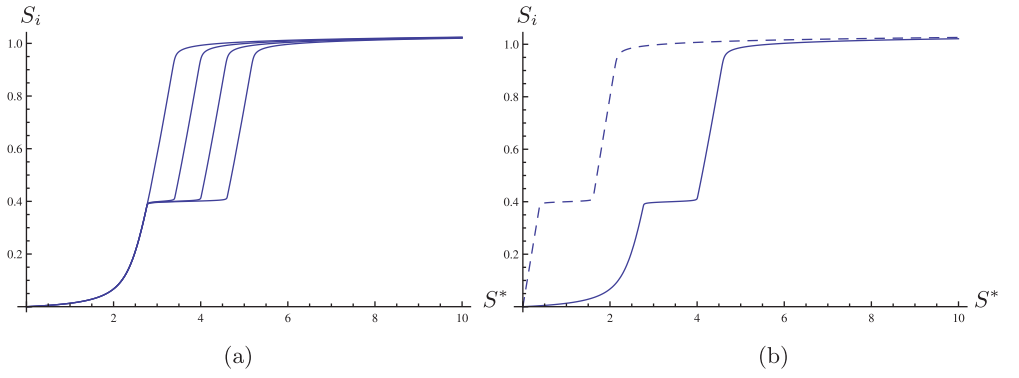

FIGURE 2. (a) Graph showing how the subsurface surfactant concentration S_i given by (3.11c) varies with bulk surfactant concentration S^* for $P^* = 0, 0.6, 1.2, 1.8$ and $\Gamma^* = 2$. (b) Graph comparing S_i versus S^* (for $P^* = 1.2$) under dynamic conditions, $\Gamma^* = 2$ (solid line), and static conditions, $\Gamma^* = 0$ (dashed line). The other parameters used were $\delta = 0.4$, $M = 200$, $N = 80$, $\beta = 0.02$.

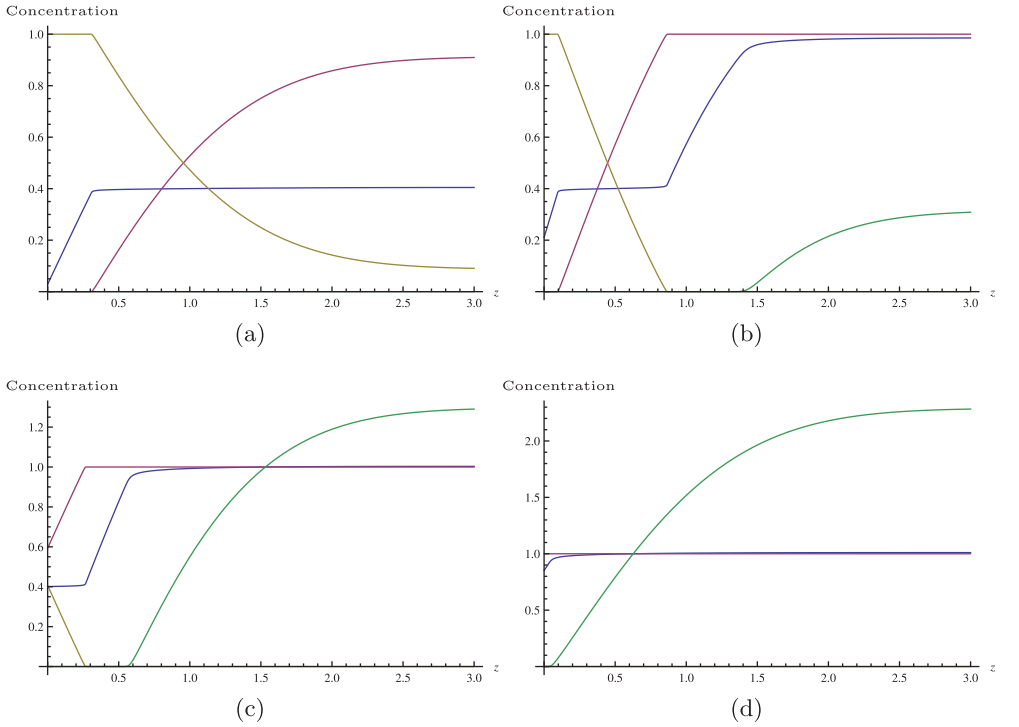

FIGURE 3. Graphs showing the variations of the surfactant concentration (blue), micelle concentration (green), polymer concentration (brown), and polymer–micelle complex concentration (red) with depth into the fluid for (a) $S^* = 1.5$, (b) $S^* = 2.5$, (c)$S^* = 3.5$, and (d) $S^* = 4.5$. The other parameters are: $P^* = 1.2$, $\delta = 0.4$, $\beta = 0.02$, $N = 80$, $M = 200$, and $\Gamma^* = 2$. For interpretation of the references to colour in this figure, the reader is referred to the online version of this article.

https://doi.org/10.1017/S0956792515000327 Published online by Cambridge University Press

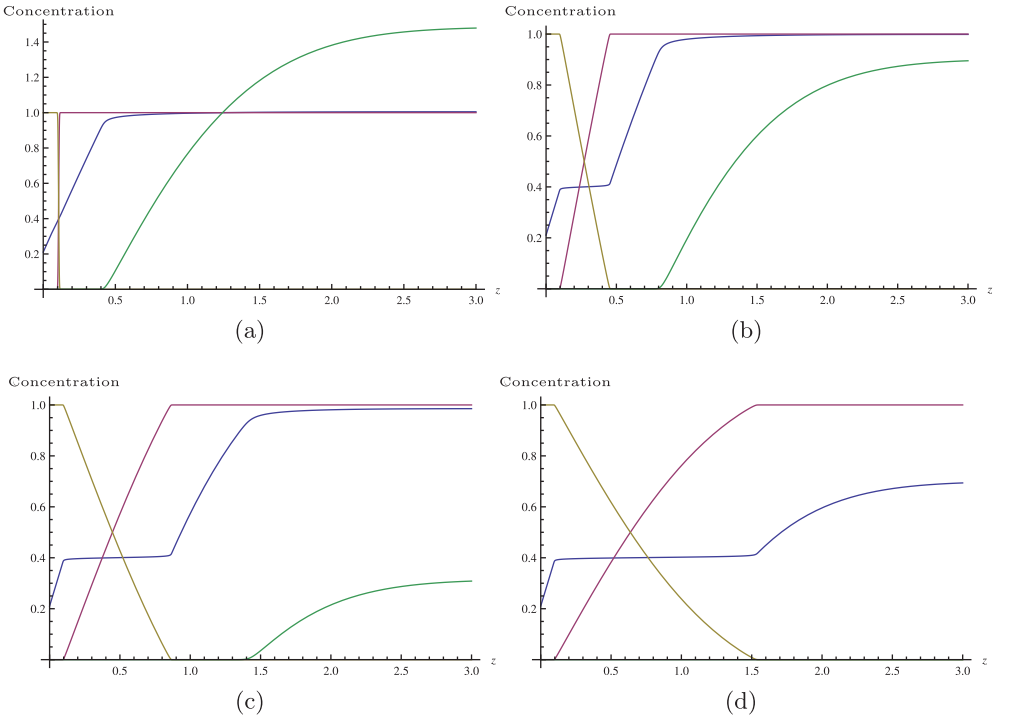

FIGURE 4. Graphs showing the variations of the surfactant concentration (blue), micelle concentration (green), polymer concentration (brown), and polymer–micelle complex concentration (red) with depth into the fluid for (a) $P^* = 0.01$, (b) $P^* = 0.6$, (c) $P^* = 1.2$, and (d) $P^* = 1.8$. The other parameters are: $S^* = 2.5$, $\delta = 0.4$, $\beta = 0.02$, $N = 80$, $M = 200$, and $\Gamma^* = 2$. For interpretation of the references to colour in this figure, the reader is referred to the online version of this article.

surface monomer concentration is below the CAC but the bulk monomer concentration is above the CAC, see Figure 3(b). Close to the free surface, we have a region devoid of complexes and the monomer concentration increases. At a certain depth, the monomer concentration reaches the CAC and beneath this depth plateaus out, complexes form, and the concentration of free polymer decreases. This continues until no free polymer remains. Travelling further away from the free surface, the monomer concentration then starts to rise again until it reaches the CMC, where it plateaus and micelles form. When the surface concentration is the same order as the CAC (Figure 3(c)), complexes are present right up to the free surface, but the behaviour of the rest of the system is the same as previously described. Finally, when the surface concentration is above the CAC, there are no free polymers anywhere in the solution, and increasing the bulk concentration increases the surface concentration up to the CMC and reduces the width of the layer devoid of micelles close to the free surface (Figure 3(d)). At even higher concentrations, micelles exist all the way up to the free surface.

It is also interesting to keep the bulk surfactant concentration constant and vary the polymer concentration (through P^*), as shown in Figure 4, where we have chosen the parameters so that the surface concentration is below the CAC. For very small values of

https://doi.org/10.1017/S0956792515000327 Published online by Cambridge University Press

P^*, we see in Figure 4(d) that there is a rapid conversion of free polymer to complex at the depth where the surfactant concentration crosses the CAC and there is no plateau in surfactant concentration at the CAC. As the concentration of polymer increases, the plateau in surfactant concentration at the CAC forms within the bulk liquid, and the size of this region increases as P^* increases. In this plateau region, complexes form as described previously. Finally, as P^* increases, the amount of surfactant available to form free micelles decreases, as can be seen in the four pictures in Figure 4, and eventually micelles are eliminated from the system. We note that the depth beneath the surface at which the surfactant concentration reaches the CAC does not change as P^* is varied.

3.1.1 *Predicting the layered structure in the concentrations*

We now aim to predict the sharp transitions in the concentration profiles seen in Figures 3 and 4, exploiting the fact that N and M are large. We let $N, M \to \infty$ with $N/M \sim O(1)$, and obtain explicit formulae for each of the concentrations between these transitions. It is useful to restate the solution given in (3.11) in the form

$$S_m = S^N, \qquad P = \frac{\delta^M}{\delta^M + S^M}, \qquad P + P_m = 1, \tag{3.12}$$

$$S + S_m + P^* P_m = S^* - \left(S^* - S_i - S_i^N - \frac{P^* S_i^M}{\delta^M + S_i^M}\right) \operatorname{erfc}\left(\frac{z}{\sqrt{2}}\right), \tag{3.13}$$

where S_i satisfies

$$S_i + S_i^N + \frac{P^* S_i^M}{\delta^M + S^M} = S^* - \sqrt{\frac{\pi}{2}} \frac{\Gamma^* S_i}{\beta + S_i}. \tag{3.14}$$

We consider the case where $S_i < \delta$, which from the previous section we see has the most structure, and where the bulk concentration $S^* > 1 + P^*$, for reasons that we will see later. In this case, close to the interface we have $P = 1$, $P_m = 0$, S_m=0, and the surface concentration can be explicitly determined since (3.14) reduces to a quadratic equation, yielding

$$S_i = \frac{1}{2}\left[S^* - \beta - \sqrt{\frac{\pi}{2}}\Gamma^* + \sqrt{\left(S^* - \beta - \sqrt{\frac{\pi}{2}}\Gamma^*\right)^2 + 4S^*\beta}\right], \tag{3.15}$$

while the surfactant concentration satisfies

$$S = S^* - (S^* - S_i) \operatorname{erfc}\left(\frac{z}{\sqrt{2}}\right), \tag{3.16}$$

which holds provided $S < \delta$. Since S increases away from the free surface, it will increase to $S = \delta$ at some distance $z = z_1$ beneath the free surface, given by

$$\operatorname{erfc}\left(\frac{z_1}{\sqrt{2}}\right) = \frac{S^* - \delta}{S^* - S_i}. \tag{3.17}$$

As we would anticipate, for there to exist a solution of (3.17) for z_1, the bulk surfactant concentration must exceed the CAC, *i.e.* we must have $S^* > \delta$. For $z > z_1$ we have a

https://doi.org/10.1017/S0956792515000327 Published online by Cambridge University Press

region where the polymer converts to complex. In this region, $S = \delta$, $S_m = 0$, and

$$P_m = \frac{1}{P^*}\left(S^* - \delta - (S^* - S_i)\ \mathrm{erfc}\left(\frac{z}{\sqrt{2}}\right)\right), \tag{3.18}$$

$$P = 1 - \frac{1}{P^*}\left(S^* - \delta - (S^* - S_i)\ \mathrm{erfc}\left(\frac{z}{\sqrt{2}}\right)\right), \tag{3.19}$$

which holds until all of the unbound polymer has bound into aggregates. We define $z = z_2$ as the place where $P = 0$, *i.e*

$$\mathrm{erfc}\left(\frac{z_2}{\sqrt{2}}\right) = \frac{S^* - P^* - \delta}{S^* - S_i}, \tag{3.20}$$

which exists providing $S^* > P^* + \delta$. For $z > z_2$, all the polymer is bound and the monomer concentration increases up to the CMC, reached at $z = z_3$, given by

$$\mathrm{erfc}\left(\frac{z_3}{\sqrt{2}}\right) = \frac{S^* - P^* - 1}{S^* - S_i}, \tag{3.21}$$

which exists for $S^* > 1 + P^*$. Between z_2 and z_3, $S_m = 0$, $P = 0$, $P_m = 1$ and

$$S = S^* - P^* - (S^* - S_i)\ \mathrm{erfc}\left(\frac{z}{\sqrt{2}}\right). \tag{3.22}$$

For $z > z_3$, the monomer concentration is at the CMC and micelles form in the bulk. Thus $S = 1$, $P = 0$, $P_m = 0$ and

$$S_m = S^* - 1 - P^* - (S^* - S_i)\ \mathrm{erfc}\left(\frac{z}{\sqrt{2}}\right). \tag{3.23}$$

Thus, providing the parameters are such that $S_i < \delta$ and $S^* > 1 + P^*$, we expect to find four distinct regions in the fluid, separated by the boundaries z_1, z_2, and z_3. In Figure 5, we show how the asymptotic solution compares with the exact solution for a particular set of parameters. We see that there is reasonable agreement between the two solutions and, in particular, the agreement between the asymptotic and exact solutions for P and P_m is better than the agreement between the solutions for S and S_m. This is to be expected, since $M > N$. The agreement between asymptotic and exact solutions improves as N and M increase; the agreement is also almost perfect when the $O(1/N)$ corrections are included (not shown).

In summary, when all the diffusivities are the same we are able to find an explicit analytic solution for the concentrations of all the components, along with a set of asymptotic solutions that match the explicit solution well.

3.2 Diffusivities different

We now suppose that the diffusivities of the surfactant, micelles, polymer, and complexes are different. We utilise the insight given in the previous section to look straight away for the boundary layer near the interface. We find that the fluxes out of the boundary layer,

https://doi.org/10.1017/S0956792515000327 Published online by Cambridge University Press

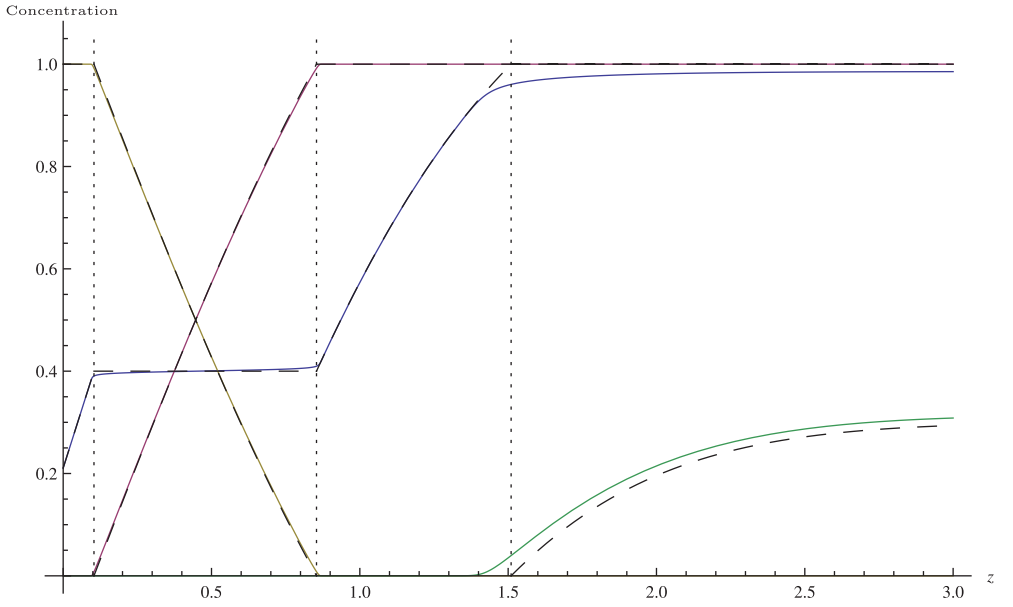

FIGURE 5. Graph showing the variations of the surfactant concentration (blue), micelle concentration (green), polymer concentration (brown), and polymer–micelle complex concentration (red) with depth into the fluid. The asymptotic solutions are overlaid using dashed lines; z_1, z_2, and z_3 are indicated as vertical dotted lines. The parameters are $P^* = 1.2$, $S^* = 2.5$, $\delta = 0.4$, $\beta = 0.02$, $N = 80$, $M = 200$, and $\Gamma^* = 2$.For interpretation of the references to colour in this figure, the reader is referred to the online version of this article.

and thus the boundary conditions on the outer problem, are

$$S' = \frac{\Gamma S_i}{\beta + S_i}\left(\frac{1}{1 + D_1 N S_i^{N-1} + \frac{D_2 D_3 P^* M P_i S_i^{M-1}}{D_2\delta^M + D_3 S_i^M}}\right), \quad D_1 S_m' = D_1 N S_i^{N-1} S', \tag{3.24}$$

$$D_2 P' = -D_2 D_3 M\left(\frac{P_i S_i^{M-1}}{D_3 S_i^M + D_2\delta^M}\right) S', \quad D_3 P_m' = D_2 D_3 M\left(\frac{P_i S_i^{M-1}}{D_3 S_i^M + D_2\delta^M}\right) S', \tag{3.25}$$

at $z = 0$, where $P_i = P(0)$. To simplify the calculation of P_m from (3.1a)[1] we introduce $Y = P + P_m$. In terms of Y,

$$P = \frac{\delta^M}{\delta^M + S^M} Y, \qquad P_m = \frac{S^M}{\delta^M + S^M} Y, \tag{3.26}$$

[1] We expect $\left(S/\delta\right)^M$ to be huge at depth (and of order $O(10^{80})$ for our parameters). At the same time, we expect $P \to 0$, and are unlikely to be able to sensibly calculate P from (3.1a) to sufficient accuracy that we can determine $P_m \sim O(1)$ with any confidence.

https://doi.org/10.1017/S0956792515000327 Published online by Cambridge University Press

while the governing equations become

$$\left(1+D_1NS^{N-1}+\frac{P^*D_3M\delta^MYS^{M-1}}{(\delta^M+S^M)^2}\right)S''+D_1N(N-1)S^{N-2}S'^2+$$

$$P^*D_3\left(\frac{2M\delta^MS^{M-1}}{(\delta^M+S^M)^2}Y'S'+\frac{S^M}{\delta^M+S^M}Y''-\frac{M\delta^MS^{M-2}\left((1+M)S^M+(1-M)\delta^M\right)Y}{(\delta^M+S^M)^3}S'^2\right)$$

$$+zS'\left(1+NS^{N-1}+\frac{P^*M\delta^MS^{M-1}Y}{(\delta^M+S^M)^2}\right)+zY'\frac{P^*S^M}{\delta^M+S^M}=0, \tag{3.27}$$

$$\left(D_3+\frac{(D_2-D_3)\delta^M}{\delta^M+S^M}\right)Y''+zY'+(D_2-D_3)\frac{M\delta^MS^{M-2}}{(\delta^M+S^M)^2}$$

$$\times\left[YS'^2\frac{\left((1+M)S^M+(1-M)\delta^M\right)}{\delta^M+S^M}-YSS''-2Y'SS'\right]=0, \tag{3.28}$$

with boundary conditions

$$Y\to 1,\qquad S\to S_\infty\qquad\text{as}\qquad z\to\infty, \tag{3.29}$$

$$S'(0)=\left(\frac{\Gamma^*S_i}{\beta+S_i}\right)\left(\frac{1}{1+D_1NS_i^{N-1}+\dfrac{D_2D_3P^*M\delta^MS_i^{M-1}Y_i}{(\delta^M+S_i^M)(D_2\delta^M+D_3S_i^M)}}\right), \tag{3.30}$$

$$Y'(0)=\frac{\dfrac{(D_2-D_3)M\delta^MS_i^{M-1}Y_i}{(\delta^M+S_i^M)(D_2\delta^M+D_3S_i^M)}\left(\dfrac{\Gamma^*S_i}{\beta+S_i}\right)}{1+D_1NS_i^{N-1}+\dfrac{D_2D_3P^*M\delta^MS_i^{M-1}Y_i}{(\delta^M+S_i^M)(D_2\delta^M+D_3S_i^M)}}, \tag{3.31}$$

where S_∞ satisfies $S_\infty+S_\infty^N+P^*S_\infty^M/(\delta^M+S_\infty^M)=S^*$, $Y_i=Y(0)$ and $S_i=S(0)$. We see immediately from (3.28), (3.29), and (3.31) that when $D_2=D_3$, $Y=1$ everywhere and (3.27) simplifies considerably.

We solve (3.26)–(3.31) numerically for various different choices of the diffusivities, and show the resulting concentration profiles in Figure 6. In the Figures 6(a) and (b), D_2=D_3 and we see that $P+P_m=1$. Comparing Figures 6(a) and (b), we also see that reducing both D_2 and D_3 by the same amount steepens the polymer and complex profiles and thus reduces the width of the region over which they adjust. We see that the subsurface surfactant concentration decreases as $D_2=D_3$ decreases and that the complexes do not get as close to the free surface. Finally, we see that reducing D_1 steepens the micelle concentration profile. When D_2 and D_3 are different, P and P_m no longer sum to one and we see that the concentration of the polymer–micelle complex develops an internal maximum which increases in magnitude as $\mathscr{D}=D_2-D_3$ increases. We also see that the subsurface concentration of *polymer* decreases as $\mathscr{D}$ increases, while the subsurface concentration of surfactant remains constant.

https://doi.org/10.1017/S0956792515000327 Published online by Cambridge University Press

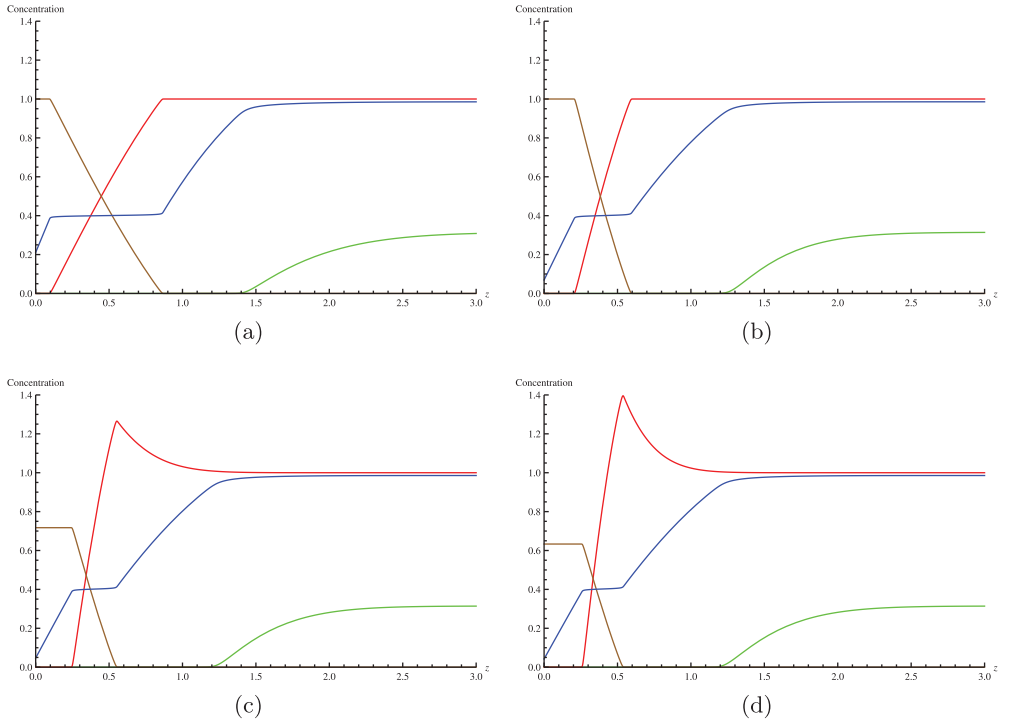

FIGURE 6. Graphs showing the variations of the surfactant concentration (blue), micelle concentration (green), polymer concentration (brown), and polymer–micelle complex concentration (red) with depth into the fluid for (a) $D_1 = D_2 = D_3 = 1$, (b) $D_1 = 0.6$, $D_2 = D_3 = 0.4$, (c) $D_1 = 0.6$, $D_2 = 0.4$, $D_3 = 0.2$, and (d) $D_1 = 0.6$, $D_2 = 0.4$, $D_3 = 0.15$. The other parameters are: $S^* = 2.5$, $\delta = 0.4$, $\beta = 0.02$, $N = 80$, $M = 200$, $\Gamma^* = 2$, and $P_s = 1.2$. For interpretation of the references to colour in this figure, the reader is referred to the online version of this article.

3.2.1 *Predicting the layered structure in the concentrations*

Following the same recipe as in Section 3.1.1, we now predict the sharp transitions in the concentrations and their shapes between these transitions. We suppose that we are operating in a situation where $S(0) = S_i < \delta$, and we let $N, M \to \infty$ with $N/M \sim O(1)$. We find that there are four regions, with the following solutions:

Region 1, $0 \leqslant z \leqslant z_1$

$$P_m = 0, \qquad S_m = 0, \qquad S = S_i + \frac{\pi}{2}\left(\frac{\Gamma^* S_i}{\beta + S_i}\right)\left(1 - \operatorname{erfc}\left(\frac{z}{\sqrt{2}}\right)\right), \tag{3.32}$$

$$P = \frac{1}{P^*}\sqrt{\frac{\pi}{2D_2}}\left(\frac{\Gamma^* S_i}{\beta + S_i}\right) e^{\frac{(1-D_2)z_1^2}{2D_2}}\left(\operatorname{erfc}\left(\frac{z_1}{\sqrt{2D_2}}\right) - \operatorname{erfc}\left(\frac{z_2}{\sqrt{2D_2}}\right)\right). \tag{3.33}$$

Region 2, $z_1 \leqslant z \leqslant z_2$

$$S_m = 0, \qquad S = \delta, \tag{3.34}$$

https://doi.org/10.1017/S0956792515000327 Published online by Cambridge University Press

$$P = \frac{1}{P^*}\sqrt{\frac{\pi}{2D_2}}\left(\frac{\Gamma^* S_i}{\beta + S_i}\right) e^{\frac{(1-D_2)z_1^2}{2D_2}}\left(\operatorname{erfc}\left(\frac{z}{\sqrt{2D_2}}\right) - \operatorname{erfc}\left(\frac{z_2}{\sqrt{2D_2}}\right)\right), \tag{3.35}$$

$$P_m = -\frac{1}{P^*}\sqrt{\frac{\pi}{2D_3}}\left(\frac{\Gamma^* S_i}{\beta + S_i}\right) e^{\frac{(1-D_3)z_1^2}{2D_3}}\left(\operatorname{erfc}\left(\frac{z}{\sqrt{2D_3}}\right) - \operatorname{erfc}\left(\frac{z_1}{\sqrt{2D_3}}\right)\right). \tag{3.36}$$

Region 3, $z_2 \leqslant z \leqslant z_3$

$$P = 0, \qquad S_m = 0, \qquad S = \delta + (1-\delta)\frac{\operatorname{erfc}\left(\frac{z}{\sqrt{2}}\right) - \operatorname{erfc}\left(\frac{z_2}{\sqrt{2}}\right)}{\operatorname{erfc}\left(\frac{z_3}{\sqrt{2}}\right) - \operatorname{erfc}\left(\frac{z_2}{\sqrt{2}}\right)}, \tag{3.37}$$

$$P_m = 1 - \left(\sqrt{\frac{\pi}{2D_3}}\left(\frac{\Gamma^* S_i}{\beta + S_i}\right) e^{\frac{(1-D_3)z_1^2}{2D_3}} + \frac{(1-\delta)e^{\frac{(1-D_3)z_2^2}{2D_3}}}{\sqrt{D_3}\left(\operatorname{erfc}\left(\frac{z_3}{\sqrt{2}}\right) - \operatorname{erfc}\left(\frac{z_2}{\sqrt{2}}\right)\right)}\right)\frac{\operatorname{erfc}\left(\frac{z}{\sqrt{2D_3}}\right)}{P^*}. \tag{3.38}$$

Region 4, $z \geqslant z_3$

$$P = 0, \qquad S = 1, \qquad S_m = \left(S^* - P^* - 1\right)\left(1 - \frac{\operatorname{erfc}\left(\frac{z}{\sqrt{2D_1}}\right)}{\operatorname{erfc}\left(\frac{z_3}{\sqrt{2D_1}}\right)}\right), \tag{3.39}$$

and P_m given again by (3.38); we note that there is no sharp transition in P_m at $z = z_3$.

The formulae for determining S_i, z_1, z_2 and z_3 are given by

$$\delta = S_i + \sqrt{\frac{\pi}{2}}\left(\frac{\Gamma^* S_i}{\beta + S_i}\right)\left(1 - \operatorname{erfc}\left(\frac{z_1}{\sqrt{2}}\right)\right), \tag{3.40}$$

$$\frac{1-\delta}{\operatorname{erfc}\left(\frac{z_3}{\sqrt{2}}\right) - \operatorname{erfc}\left(\frac{z_2}{\sqrt{2}}\right)} = -\frac{\sqrt{D_1}\left(S^* - P^* - 1\right)}{\operatorname{erfc}\left(\frac{z_3}{\sqrt{2D_1}}\right)} e^{\frac{-(1-D_1)z_3^2}{2D_1}}, \tag{3.41}$$

$$\sqrt{\frac{\pi}{2}}\left(\frac{\Gamma^* S_i}{\beta + S_i}\right) e^{\frac{(1-D_2)z_1^2}{2D_2}} e^{-\frac{z_2^2}{2D_2}} = -\frac{(1-\delta)e^{-\frac{z_2^2}{2}}}{\operatorname{erfc}\left(\frac{z_3}{\sqrt{2}}\right) - \operatorname{erfc}\left(\frac{z_2}{\sqrt{2}}\right)}, \tag{3.42}$$

$$\frac{1}{P^*}\sqrt{\frac{\pi}{2D_3}}\left(\frac{\Gamma^* S_i}{\beta + S_i}\right) e^{\frac{(1-D_3)z_1^2}{2D_3}} \operatorname{erfc}\left(\frac{z_1}{\sqrt{2D_3}}\right) = 1 - \frac{1-\delta}{P^*\sqrt{D_3}}\left(\frac{e^{\frac{(1-D_3)z_2^2}{2D_3}} \operatorname{erfc}\left(\frac{z_2}{\sqrt{2D_3}}\right)}{\operatorname{erfc}\left(\frac{z_3}{\sqrt{2}}\right) - \operatorname{erfc}\left(\frac{z_2}{\sqrt{2}}\right)}\right). \tag{3.43}$$

In contrast with the relationships given in Section 3.1.1, here we have to solve coupled equations for S_i, z_1, z_2, and z_3. In Figure 7, we show how the asymptotic solution compares with the numerical solution and we (again) see reasonable agreement between the two.

https://doi.org/10.1017/S0956792515000327 Published online by Cambridge University Press

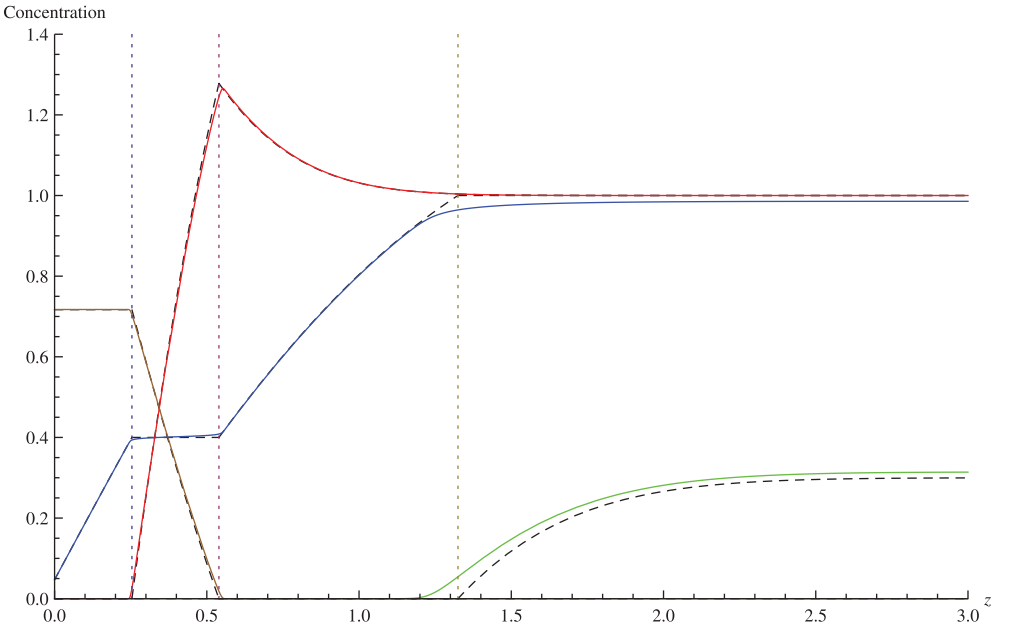

FIGURE 7. Graph showing the variations of the surfactant concentration (blue), micelle concentration (green), polymer concentration (brown), and polymer–micelle complex concentration (red) with depth into the fluid. The asymptotic solutions are overlaid using dashed lines; z_1, z_2, and z_3 are indicated as vertical dotted lines. The parameters are: $P^* = 1.2$, $S^* = 2.5$, $\delta = 0.4$, $\beta = 0.02$, $N = 80$, $M = 200$, $\Gamma^* = 2$, $D_1 = 0.6$, $D_2 = 0.4$, and $D_3 = 0.2$.For interpretation of the references to colour in this figure, the reader is referred to the online version of this article.

4 $O(1)$ reaction rates K_0 and K_1 and aggregation numbers N and M

In this section, we consider the situation when the reaction rates are $O(1)$. In this case, we solve the full system (2.14*a*)–(2.14*f*) numerically using the Chebfun package for MATLAB and using numerical continuation to increase the values of N and M. We show the results as the reaction rates and aggregation numbers are altered in Figure 8. We see that for the moderate values of the K_1 shown, all four species are present right up to the free surface. As the aggregation numbers are increased, away from the free surface the profiles tend to the large K_0, K_1, large N, M limit. However, close to the free surface this is not the case and this motivates us to consider the asymptotic limit of finite K_0 and K_1 and infinite N, M.

4.1 N, M large, aggregation numbers $O(1)$

As N and M increase, the system (2.14) becomes extremely stiff and numerical solution is practically impossible for realistic values $N, M \gtrsim 50$. To probe the behaviour for physically relevant values, it is therefore necessary to consider the asymptotic limit where $N, M \to \infty$. In this asymptotic limit, there are three main regions of interest, where $S < \delta$, $\delta < S < 1$ and $S \sim 1$; the plateau in which $S = \delta$ is no longer present. As previously, we consider the case where $S_i < \delta$, and assume (again) that the surfactant concentration reaches $S = \delta$ at some distance $z = z_1$ beneath the surface.

https://doi.org/10.1017/S0956792515000327 Published online by Cambridge University Press

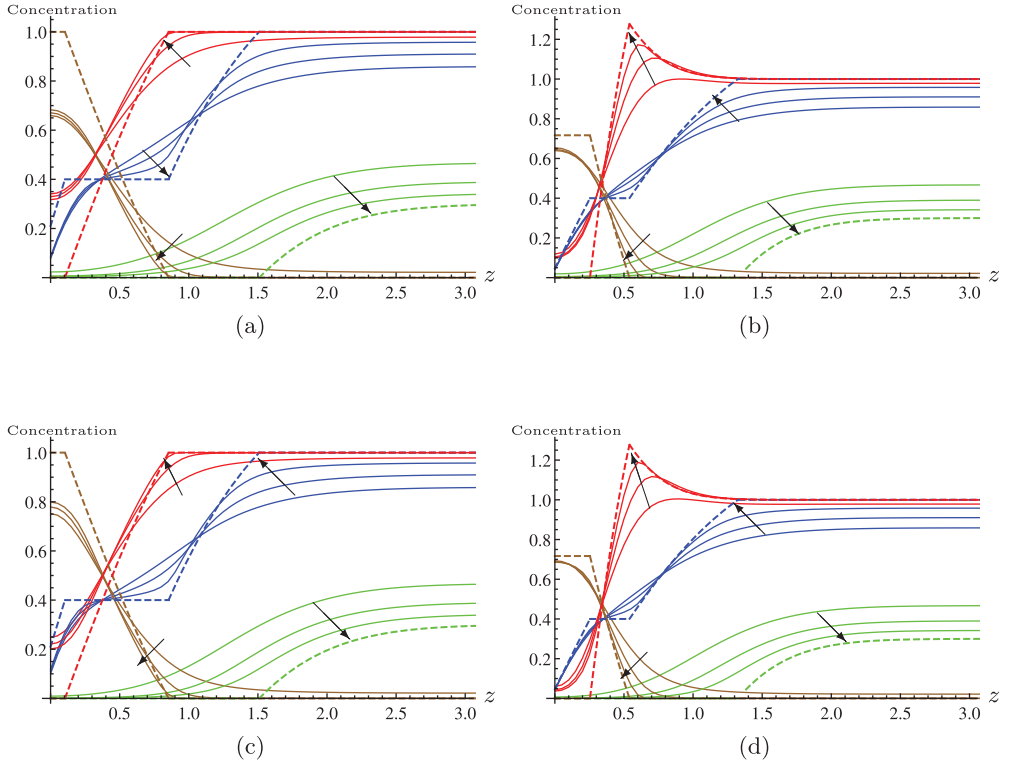

FIGURE 8. Graphs showing the variations of the surfactant concentration (blue), micelle concentration (green), polymer concentration (brown), and polymer–micelle complex concentration (red) with depth into the fluid for $N = M = 5$, 10, 25 when (a) $K_0 = K_1 = 10$ and $D_1 = D_2 = D_3 = 1$, (b) $K_0 = K_1 = 10$ and $D_1 = 0.6$, $D_2 = 0.4$, $D_3 = 0.2$, (c) $K_0 = K_1 = 20$ and $D_1 = D_2 = D_3 = 1$, (d) $K_0 = K_1 = 20$ and $D_1 = 0.6$, $D_2 = 0.4$, $D_3 = 0.2$. The arrows show the direction of increasing N, M, and the large N, M, K_0 and K_1 asymptotic solutions are shown as dashed lines. The other parameters are: $S^* = 2.5$, $\delta = 0.4$, $\beta = 0.02$, $\Gamma^* = 2$, and $P_s = 1.2$. The arrows show the direction of increasing N and M.For interpretation of the references to colour in this figure, the reader is referred to the online version of this article.

Region 1, $0 \leqslant z \leqslant z_1$

In the region $0 \leqslant z \leqslant z_1$, S^N and $(S/\delta)^M$ are both negligible (they are exponentially small) and the equations reduce to:

$$S'' + zS' = -K_0 S_m - K_1 P^* P_m, \tag{4.1a}$$

$$D_1 S_m'' + zS_m' = K_0 S_m, \tag{4.1b}$$

$$D_2 P'' + zP' = -K_1 P_m, \tag{4.1c}$$

$$D_3 P_m'' + zP_m' = K_1 P_m, \tag{4.1d}$$

which we can solve along with the boundary conditions given in (2.14*f*) to give

$$S_m(z) = A_1 \Phi\left(K_0; z/\sqrt{2D_1}\right), \tag{4.2}$$

$$P_m(z) = C_1 \Phi\left(K_1; z/\sqrt{2D_3}\right), \tag{4.3}$$

https://doi.org/10.1017/S0956792515000327 Published online by Cambridge University Press

where Φ is shorthand for the function

$$\Phi(K;z) = \mathrm{e}^{-z^2}\,{}_1\mathrm{F}_1\left(\frac{1+K}{2}, \frac{1}{2}, z^2\right), \tag{4.4}$$

(where ${}_1F_1$ is a hypergeometric function) and

$$P = P_i - K_1\sqrt{\frac{\pi}{2D_2}}\int_0^z \left(\mathrm{erf}\left(\frac{z}{\sqrt{2D_2}}\right) - \mathrm{erf}\left(\frac{\zeta}{\sqrt{2D_2}}\right)\right) e^{\zeta^2/2D_2} P_m(\zeta)\,d\zeta, \tag{4.5}$$

$$S = S_i + \sqrt{\frac{\pi}{2}}\left(\frac{\Gamma^* S_i}{\beta + S_i}\,\mathrm{erf}\left(\frac{z}{\sqrt{2}}\right)\right.$$

$$\left. - \int_0^z \left(\mathrm{erf}\left(\frac{z}{\sqrt{2}}\right) - \mathrm{erf}\left(\frac{\zeta}{\sqrt{2}}\right)\right) e^{\zeta^2/2} \left(K_0 S_m(\zeta) + K_1 P^* P_m(\zeta)\right) d\zeta\right). \tag{4.6}$$

By considering the boundary layer connecting the region $S < \delta$ and $\delta < S < 1$ (see Appendix B), we find that all the concentrations are continuous, the micelle flux is continuous and the net flux of surfactant and polymer are also continuous. We thus have at $z = z_1$

$$[S_m] = [P_m] = \left[S_m'\right] = \left[S' - P^* D_2 P'\right] = \left[D_2 P' + D_3 P_m'\right] = 0, \quad S = \delta, \quad P = 0, \tag{4.7}$$

where $[\cdot]$ denotes the change as we cross $z = z_1$.

Region 2, $z_1 \leqslant z \leqslant z_3$

In the region $\delta < S < 1$, S^N is still negligible but $(S/\delta)^M$ has become exponentially large. We conclude that P is exponentially small and the concentrations of the other species satisfy

$$S'' + zS' = -K_0 S_m, \tag{4.8a}$$

$$D_1 S_m'' + zS_m' = K_0 S_m, \tag{4.8b}$$

$$D_3 P_m'' + zP_m' = 0. \tag{4.8c}$$

These equations hold until $z = z_3$, where $S = 1$. Before solving in this region, let us consider the third region.

Region 3, $z \geqslant z_3$

When $z > z_3$, we still have $P = 0$ but now S is close to one and so we write $S = 1 + \phi/N$. The resulting equations become

$$\frac{1}{N}\left(\phi'' + z\phi'\right) = -K_0\left(S_m - S^N\right), \tag{4.9a}$$

$$D_1 S_m'' + zS_m' = -\frac{1}{N}\left(\phi'' + z\phi'\right), \tag{4.9b}$$

$$D_3 P_m'' + zP_m' = 0. \tag{4.9c}$$

https://doi.org/10.1017/S0956792515000327 Published online by Cambridge University Press

Thus, to leading order in $1/N$, the solution in $z > z_3$ is

$$P = 0, \quad S = 1, \quad S_m = S^* - P^* - 1 + A_3 \operatorname{erfc}\left(\frac{z}{\sqrt{2D_1}}\right), \quad P_m = 1 + B_2 \operatorname{erfc}\left(\frac{z}{\sqrt{2D_3}}\right), \tag{4.10}$$

where A_3 and B_2 are integration constants. By considering the boundary layer at $z = z_3$ (see Appendix B), we find that the concentrations of S, S_m, and P_m are all smooth at $z = z_3$.

Returning to consider the solution in region 2, we note that, since P_m is smooth at $z = z_3$ and S_m is smooth at $z = z_1$,

$$S_m = A_1 \Phi\left(K_0; \frac{z}{\sqrt{2D_1}}\right), \qquad P_m = 1 + B_2 \operatorname{erfc}\left(\frac{z}{\sqrt{2D_3}}\right), \tag{4.11}$$

in region 2. We solve (4.8*a*) for S, remembering that the continuity of S and S' at $z = z_3$ give the conditions $S = 1$, $S' = 0$ at $z = z_3$, to find that

$$S(z) = 1 - K_0\sqrt{\frac{\pi}{2}} \int_z^{z_3} S_m(\xi) \mathrm{e}^{\xi^2/2} \left[\operatorname{erf}\left(\frac{\xi}{\sqrt{2}}\right) - \operatorname{erf}\left(\frac{z}{\sqrt{2}}\right)\right] \mathrm{d}\xi. \tag{4.12}$$

We are thus left with determining the remaining eight unknowns A_1, A_3, B_2, C_1, z_1, z_3, P_i, and S_i. From the smoothness of S_m at $z = z_3$ we can solve for A_1 and A_3:

$$A_1 = \frac{S^* - 1 - P^*}{\Phi\left[K_0; \dfrac{z_3}{\sqrt{2D_1}}\right] + \dfrac{\sqrt{\pi}}{2} \mathrm{e}^{z_3^2/2D_1} \operatorname{erfc}\left[\dfrac{z_3}{\sqrt{2D_1}}\right] \Phi'\left[K_0; \dfrac{z_3}{\sqrt{2D_1}}\right]}, \tag{4.13}$$

$$A_3 = -\frac{A_1\sqrt{\pi}}{2} \mathrm{e}^{z_3^2/2D_1} \Phi'\left[K_0; \frac{z_3}{\sqrt{2D_1}}\right]. \tag{4.14}$$

Similarly, the boundary conditions for P_m and P_m' at $z = z_1$ provide expressions for C_1 and B_2, namely:

$$C_1 = \left\{\sqrt{\pi} \operatorname{erfc}\left[\frac{z_1}{\sqrt{2D_3}}\right] \mathrm{e}^{z_1^2/2D_3} \left(-K_1\sqrt{\frac{D_2}{D_3}} \mathrm{e}^{-z_1^2/2D_2} I_1\left[K_1; \sqrt{\frac{D_2}{D_3}}; \frac{z_1}{\sqrt{2D_2}}\right] + \frac{1}{2}\Phi'\left[K_1; \frac{z_1}{\sqrt{2D_3}}\right]\right) + \Phi\left[K_1; \frac{z_1}{\sqrt{2D_3}}\right]\right\}^{-1}, \tag{4.15}$$

$$B_2 = -C_1\sqrt{\pi} \mathrm{e}^{z_1^2/2D_3} \left(-K_1\sqrt{\frac{D_2}{D_3}} \mathrm{e}^{-z_1^2/2D_2} I_1\left[K_1; \sqrt{\frac{D_2}{D_3}}; \frac{z_1}{\sqrt{2D_2}}\right] + \frac{1}{2}\Phi'\left[K_1; \frac{z_1}{\sqrt{2D_3}}\right]\right), \tag{4.16}$$

where we have introduced shorthand for the following integrals:

$$I_1[K; r; z] = \int_0^z \Phi(K; r\xi) \mathrm{e}^{\xi^2} \mathrm{d}\xi, \qquad I_2[K; r; z] = \int_0^z \Phi(K; r\xi) \operatorname{erf}(\xi) \mathrm{e}^{\xi^2} \mathrm{d}\xi. \tag{4.17}$$

https://doi.org/10.1017/S0956792515000327 Published online by Cambridge University Press

We can determine S_i and P_i from the conditions $S(z_1) = \delta$ and $P(z_1) = 0$:

$$S_i + \frac{\Gamma^* S_i}{\beta + S_i}\sqrt{\frac{\pi}{2}}\ \mathrm{erf}\left(\frac{z_1}{\sqrt{2}}\right) = \delta + K_0 A_1 \sqrt{\pi}\left(\mathrm{erf}\left[\frac{z_1}{\sqrt{2}}\right] I_1\left[K_0; \frac{1}{\sqrt{D_1}}; \frac{z_1}{\sqrt{2}}\right] - I_2\left[K_0; \frac{1}{\sqrt{D_1}}; \frac{z_1}{\sqrt{2}}\right]\right) + P^* K_1 C_1 \sqrt{\pi}\left(\mathrm{erf}\left[\frac{z_1}{\sqrt{2}}\right] I_1\left[K_1; \frac{1}{\sqrt{D_3}}; \frac{z_1}{\sqrt{2}}\right] - I_2\left[K_1; \frac{1}{\sqrt{D_3}}; \frac{z_1}{\sqrt{2}}\right]\right), \quad (4.18)$$

$$P_i = K_1 C_1 \sqrt{\pi}\left(\mathrm{erf}\left[\frac{z_1}{\sqrt{2D_2}}\right] I_1\left[K_1; \sqrt{\frac{D_2}{D_3}}; \frac{z_1}{\sqrt{2D_2}}\right] - I_2\left[K_1; \sqrt{\frac{D_2}{D_3}}; \frac{z_1}{\sqrt{2D_2}}\right]\right). \quad (4.19)$$

The condition $S(z_1) = \delta$ also leads to

$$1 - \delta = K_0 A_1 \sqrt{\pi}\left\{I_2\left[K_0; \frac{1}{\sqrt{D_1}}; \frac{z_3}{\sqrt{2}}\right] - I_2\left[K_0; \frac{1}{\sqrt{D_1}}; \frac{z_1}{\sqrt{2}}\right] - \mathrm{erf}\left[\frac{z_1}{\sqrt{2}}\right]\left(I_1\left[K_0; \frac{1}{\sqrt{D_1}}; \frac{z_3}{\sqrt{2}}\right] - I_1\left[K_0; \frac{1}{\sqrt{D_1}}; \frac{z_1}{\sqrt{2}}\right]\right)\right\}. \quad (4.20)$$

Finally, the condition $[S' - P^* D_2 P'] = 0$ at $z = z_1$ gives

$$\frac{\Gamma^* S_i}{\beta + S_i} = K_0 A_1 \sqrt{2} I_1\left[K_0; \frac{1}{\sqrt{D_1}}; \frac{z_3}{\sqrt{2}}\right] + P^* K_1 C_1\left(\sqrt{2} I_1\left[K_1; \frac{1}{\sqrt{D_3}}; \frac{z_1}{\sqrt{2}}\right] - \sqrt{2D_2}\, \mathrm{e}^{-(1-D_2)z_1^2/2D_2} I_1\left[K_1; \sqrt{\frac{D_2}{D_3}}; \frac{z_1}{\sqrt{2D_2}}\right]\right). \quad (4.21)$$

Given values of the parameters K_0, K_1, D_1, D_2, D_3, δ, Γ^*, β, S^*, and P^*, we have to solve the three coupled non-linear algebraic equations (4.18), (4.20) and (4.21) for S_i, z_1, and z_3. Then P_i is determined *a posteriori* from the decoupled equation (4.19). In Figure 9, we compare the asymptotic solution presented in this section with the equivalent numerical solution. We find from the asymptotics that $S_i \approx 0.022$, $z_1 \approx 0.49$ and $z_3 \approx 2.06$. It is evident that the main qualitative features of the numerical solutions are well reflected in these approximate solutions. In particular, we observe the local maximum in the concentration of the polymer-surfactant complex coincides with a kink in the profile of the surfactant concentration.

5 Conclusions

In this paper, we have considered the straining flow of a weakly interacting polymer–surfactant system and have combined and expanded our previous work on static polymer–surfactant systems presented in Bell et al. [5] and on dynamic surfactant systems presented in Breward and Howell [8]. We assumed that the surfactant is able to exist as monomer, in micelles, and in polymer–micelle aggregates. We wrote down a model for the concentration of each of these species and of free polymer, assuming a straining flow towards a static free surface.

https://doi.org/10.1017/S0956792515000327 Published online by Cambridge University Press

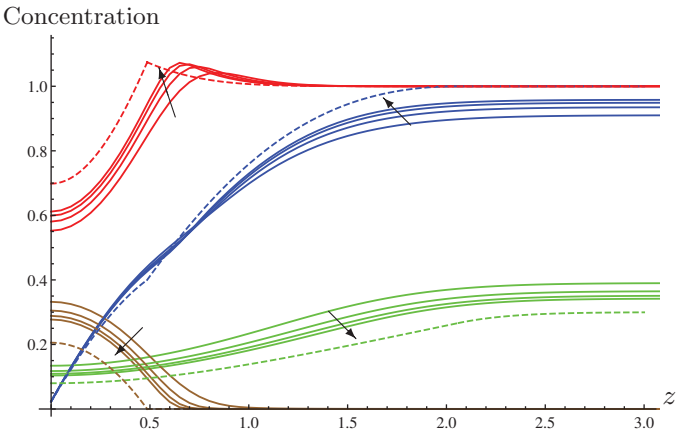

FIGURE 9. Graph showing concentrations of surfactant (blue), micelles (green), polymer (brown), and polymer–surfactant complex (red) versus depth for $N = M = 5$, 10, 15 and 20. The arrows show the direction of increasing N and M, and the dashed lines show the asymptotic solution as $N, M \to \infty$. The other parameters are $P^* = 1.2$, $S^* = 2.5$, $\delta = 0.4$, $\beta = 0.02$, $\Gamma^* = 2$, $D_1 = 0.6$, $D_2 = 0.4$, $D_3 = 0.2$, $K_0 = K_1 = 1$.For interpretation of the references to colour in this figure, the reader is referred to the online version of this article.

In the limit of large reaction rates, we reduced the system of four coupled ODEs for the concentrations of surfactant, polymer, polymer–micelle aggregates, and micelles to a pair of ODEs, which are coupled with two algebraic expressions. To simplify the problem further, we first considered the case where the diffusivities of each of the four species are the same. In this case, we found that there is a small boundary layer, of thickness $1/\sqrt{K_1}$, over which the concentration of polymer, micelles and complexes adjusts to ensure no flux of these species onto the free surface. In considering this boundary layer calculation, we were able to resolve an outstanding question from the earlier work [8], namely what happens to the subsurface concentration as it approaches the CMC, and update a formula given there so that it is correct for all subsurface concentrations. We showed how the subsurface surfactant concentration varies with the bulk surfactant concentration for various concentrations of polymer. We further illustrated how the presence of the flow alters these profiles when compared with the static case. The key observation was that much less surfactant reaches the interface when the system is dynamic. We looked at the distribution of each of the species beneath the free surface, and we found that, for bulk concentrations just above the CMC, a region devoid of micelles and complexes forms beneath the free surface. This is because the straining flow causes the surface concentration to be beneath both the CAC and the CMC, and all the micelles and complexes approaching the free surface have to break down in order to supply the required surface adsorption. Beneath the surface, the surfactant concentration increases to the CAC and then a plateau region forms where the concentration does not change but complexes start to form. Once all the polymer has formed complexes, the surfactant concentration rises to the CMC, and beyond this depth, micelles start to form. Using asymptotic analysis in the limit of large aggregation numbers N and M, we were able to decompose the domain into four regions and derive simple expressions for the concentrations of each of the species;

https://doi.org/10.1017/S0956792515000327 Published online by Cambridge University Press

these asymptotic expressions matched well with the explicit solutions to this reduced problem.

When the diffusivities differ, the solution structure remains the same but the equations are more complicated. We solved these numerically to find how the concentrations vary with depth from the free surface, and were again able to derive asymptotic solutions in the limit of large aggregation numbers, which provide a simpler formula for each of the concentrations. The main difference between the solution with identical diffusivities and the solution with different diffusivities is that the total polymer concentration (that is, the sum of the amount of free polymer and polymer bound in aggregates) at any given depth is not constant. We found that a maximum in the concentration of polymer–micelle aggregates forms in the bulk fluid, and that the magnitude of this maximum increases as the diffusivity of the aggregates decreases (with the knock-on effect that less polymer reaches the interface). Given that polymer is added to the system in order to alter the viscosity, it is interesting to note that the results suggest it will be least effective at doing so near the free surface.

Of course, in practice the reaction rates will be finite and so we also solved the full (1-D) problem numerically with all parameters finite. We found that all species are present throughout the fluid although, as in the previous case, the micelles and complexes are depleted near the free surface. We again saw that the overall polymer concentration is depleted near the free surface when the diffusivity of the complexes is reduced. We looked for another asymptotic limit in which the aggregation numbers N and M are taken to infinity but the reaction rates kept finite. We found that the domain decomposes into three regions rather than four – the plateau found in the infinite reaction rate case is not present when the rates are finite. The asymptotics predict a kink in the concentration of surfactant, which occurs at the same depth as the maximum in the concentration of complex, and these asymptotics agree with numerical simulation.

One key limitation of the work described in this paper is that we limited ourselves to concentration variations perpendicular to the free surface. In future work, we intend to investigate whether the 1-D layered structure is stable to transverse perturbations.

We are unaware of any experimental data on straining flows of polymer–surfactant systems, and we hope that these results will provide a catalyst to our experimental colleagues to investigate these systems under dynamic conditions. In particular, in the future we hope that we could fit our model to experimental data for the surface concentration of surfactant (which can be extracted from surface tension or surface excess data) and then use our model to help determine the rate parameter K_1[2]. Our key goal for the future is to use the insight we have gained from this modelling study to help understand other polymer–surfactant flows where the fluid mechanics is affected by the surfactant distribution at the surface, and vice versa.

[2] The rate parameter K_0 can be determined by matching the model with polymer-free data, as shown in Breward and Howell [8].

https://doi.org/10.1017/S0956792515000327 Published online by Cambridge University Press

Acknowledgements

We are grateful to Colin Bain for many fruitful discussions about the overflowing cylinder, and to Jeff Penfold and Bob Thomas for guiding our investigations of polymer–surfactant systems. This work would not have been possible if John Ockendon had not encouraged us to start working on surfactant-driven flows twenty years ago, and we are indebted to him for this (and for many other things).

Part of this work was supported by an EPSRC CASE award with the Rutherford Appleton Laboratory.

Appendix A Boundary layers near the free surface

In this appendix we look in more detail at the boundary layer structure beneath the interface that arises when the reaction rates K_0 and K_1 are large. We illustrate the calculation in the case where the diffusivities are the same and there are no micelles present. The calculations when the diffusivities are different and when micelles are present are simple extensions. The outer solution is given by (3.4) and the micelle-free versions of (3.5), namely

$$P = \frac{\delta^M}{\delta^M + S^M}\left(1 + b\ \mathrm{erfc}\left(\frac{z}{\sqrt{2}}\right)\right), \qquad P_m = \frac{S_M}{\delta^M + S^M}\left(1 + b\ \mathrm{erfc}\left(\frac{z}{\sqrt{2}}\right)\right), \quad \text{(A 1)}$$

$$S + P^*\frac{S^M}{\delta^M + S^M}\left(1 + b\ \mathrm{erfc}\left(\frac{z}{\sqrt{2}}\right)\right) = S^* + a\ \mathrm{erfc}\left(\frac{z}{\sqrt{2}}\right). \quad \text{(A 2)}$$

The limit of these outer solutions as $z \to 0$ is:

$$S' = \frac{\sqrt{\frac{2}{\pi}}\left(\frac{P^* S^M}{\delta^M + S^M}b - a\right)}{1 + \frac{P^* M \delta^M S^{M-1}(1+b)}{\left(\delta^M + S^M\right)^2}}, \quad \text{(A 3)}$$

$$P' = -\frac{\delta^M}{\delta^M + S^M}\sqrt{\frac{2}{\pi}}b - \frac{M\delta^M S^{M-1}(1+b)}{(\delta^M + S^M)^2}S', \quad \text{(A 4)}$$

$$P_m' = -\frac{S^M}{\delta^M + S^M}\sqrt{\frac{2}{\pi}}b + \frac{M\delta^M S^{M-1}(1+b)}{(\delta^M + S^M)^2}S'. \quad \text{(A 5)}$$

Equations (A 3)–(A 5) clearly do not satisfy the boundary conditions $P' = P_m{}' = 0$ at $z = 0$. We thus seek a boundary layer near to the free surface. Denoting $\varepsilon = 1/\sqrt{K_1}$, we set $z = \varepsilon\xi$ and we find that the equations in the inner region become

$$S_{\xi\xi} + \varepsilon^2 S_\xi = P^*\left(P\left(S/\delta\right)^M - P_m\right), \quad \text{(A 6)}$$

$$P_{\xi\xi} + \varepsilon^2 P_\xi = \left(P\left(S/\delta\right)^M - P_m\right), \quad \text{(A 7)}$$

$$P_{m\xi\xi} + \varepsilon^2 P_{m\xi} = -\left(P\left(S/\delta\right)^M - P_m\right). \quad \text{(A 8)}$$

https://doi.org/10.1017/S0956792515000327 Published online by Cambridge University Press

The boundary conditions at $\xi = 0$ become

$$P_\xi = P_{m\xi} = 0, \qquad S_\xi = \varepsilon \frac{\Gamma^* S}{\beta + S}. \tag{A 9}$$

We can simplify the system of equations (correct to $O(\varepsilon)$) by dropping the $O(\varepsilon^2)$ terms in (A 6)–(A 8), combining, integrating and applying the boundary conditions to give

$$P + P_m = E, \qquad S + P^* P_m = \varepsilon \frac{\Gamma^* S}{\beta + S} \xi + B, \tag{A 10}$$

where E and B are constants of integration. We now expand the inner variables as asymptotic series using $S = S_0 + \varepsilon S_1 + \cdots$, $P = P_0 + \varepsilon P_1 + \cdots$, and $P = P_{m0} + \varepsilon P_{m1} + \cdots$, where S_0 is a constant. We also expand the constants of integration B and E in the same way. The leading-order problem becomes

$$P_0 + P_{m0} = E_0, \qquad S_0 + P^* P_{m0} = B_0, \qquad P_0 \left(\frac{S_0}{\delta} \right)^M = P_{m0}, \tag{A 11}$$

which has solution

$$P_0 = \frac{E_0 \delta^M}{\delta^M + S_0^M}, \qquad P_{m0} = \frac{E_0 S_0^M}{\delta^M + S_0^M}, \qquad S_0 = B_0 - \frac{P^* E_0 S_0^M}{\delta^M + S_0^M}. \tag{A 12}$$

The $O(\varepsilon)$ problem reads

$$P_1 + P_{m1} = E_1, \quad S_1 + P^* P_{m1} = \frac{\Gamma^* S_0}{\beta + S_0} \xi + B_1, \tag{A 13}$$

$$S_{1\xi\xi} = P^* \left(P_1 \left(S_0/\delta \right)^M + M \frac{P_0 S_0^{M-1}}{\delta^M} S_1 - P_{m1} \right). \tag{A 14}$$

The equation for S_1 can be written as

$$S_{1\xi\xi} = \lambda_1^2 S_1 + \lambda_2 + \lambda_3 \xi, \tag{A 15}$$

where

$$\lambda_1^2 = 1 + \frac{S_0^m}{\delta^M} + \frac{P^* E_0 M S_0^{M-1}}{\delta^M + S_0^M}, \quad \lambda_2 = \left(P^* E_1 - B_1 \right) \frac{S_0^M}{\delta^M} - B_1,$$
$$\lambda_3 = -\frac{\Gamma^* S_0}{\beta + S_0} \left(\frac{\delta^M + S_0^M}{\delta^M} \right). \tag{A 16}$$

The solution that matches with the outer and satisfies the boundary condition at $z = 0$ is

$$S_1 = -\left(\frac{\Gamma^* S_0}{\lambda_1 (\beta + S_0)} + \frac{\lambda_3}{\lambda_1^3} \right) e^{-\lambda_1 \xi} - \frac{\lambda_2 + \lambda_3 \xi}{\lambda_1^2}, \tag{A 17}$$

and thus

$$P_1 = E_1 - \frac{1}{P^*} \left[\left(\frac{\Gamma^* S_0}{\lambda_1 (\beta + S_0)} + \frac{\lambda_3}{\lambda_1^3} \right) e^{-\lambda_1 \xi} - \frac{\lambda_2 + \lambda_3 \xi}{\lambda_1^2} - B_1 - \frac{\Gamma^* S_0}{\beta + S_0} \xi \right], \tag{A 18}$$

https://doi.org/10.1017/S0956792515000327 Published online by Cambridge University Press

$$P_{m1} = \frac{1}{P^*}\left[\frac{\Gamma^* S_0}{\beta + S_0}\xi + B_1 + \left(\frac{\Gamma^* S_0}{\lambda_1(\beta + S_0)} + \frac{\lambda_3}{\lambda_1^3}\right)e^{-\lambda_1\xi} + \frac{\lambda_2 + \lambda_3\xi}{\lambda_1^2}\right]. \tag{A 19}$$

We now match with the outer solution. Matching the leading-order terms, we find that

$$S_0 = S_i, \qquad P_0 = \frac{\delta^M(1+b)}{\delta^M + S_i^M}, \qquad P_{m0} = \frac{S_i^M(1+b)}{\delta^M + S_i^M}, \tag{A 20}$$

where (as before) S_i is the "outer" $S(0)$, and thus we must have $E_0 = 1 + b$. Matching the two-term inner expansions of the one-term outer solutions with the one-term outer expansions of the two-term inner solutions, gives

$$S'(0) = \frac{\Gamma^* S_0}{\beta + S_0}\left(\frac{\delta^M + S_0^M}{\delta^M + S_0^M + \frac{ME_0P^*\delta^M S_0^{M-1}}{\delta^M + S_0^M}}\right), \quad P'(0) = -S'(0)\frac{ME_0\delta^M S_0^{M-1}}{(\delta^M + S_0^M)^2}, \tag{A 21}$$

and thus comparing (A 3) and (A 4) with (A 21) we find that

$$b = 0, \qquad a = -\sqrt{\frac{\pi}{2}}\left(\frac{\Gamma^* S_i}{\beta + S_i}\right). \tag{A 22}$$

Thus the leading-order outer solution is

$$P = \frac{\delta^M}{\delta^M + S^M}, \quad P_m = \frac{S^M}{\delta^M + S^M}, \quad S + \frac{P^* S^M}{\delta^M + S^M} = S^* - \sqrt{\frac{\pi}{2}}\left(\frac{\Gamma^* S_i}{\beta + S_i}\right)\operatorname{erfc}\left(\frac{z}{\sqrt{2}}\right), \tag{A 23}$$

where S_i is given by

$$S_i + \frac{P^* S_i^M}{\delta^M + S_i^M} = S^* - \sqrt{\frac{\pi}{2}}\left(\frac{\Gamma^* S_i}{\beta + S_i}\right). \tag{A 24}$$

Appendix B Boundary layers with $O(1)$ reaction rates

Now we look for a boundary layer model that applies in a neighbourhood of $z = z_1$ and can match with the solutions in regions 1 and 2. We rescale the variables as follows:

$$z = z_1 + M^{-1}\zeta, \tag{B 1a}$$

$$S(z) = \delta\left(1 + 2M^{-1}\log M + M^{-1}\tilde{S}(\zeta)\right), \tag{B 1b}$$

$$S_m(z) = S_m(z_1) + M^{-1}\zeta S_m'(z_1) + M^{-2}\tilde{S}_m(\zeta), \tag{B 1c}$$

$$P(z) = M^{-1}\tilde{P}(\zeta), \tag{B 1d}$$

$$P_m(z) = P_m(z_1) + M^{-1}\tilde{P}_m(\zeta), \tag{B 1e}$$

where, for simplicity of presentation, we have anticipated the result that the outer solutions for S_m, S_m', and P_m are continuous at $z = z_1$. At leading order, the governing equations

https://doi.org/10.1017/S0956792515000327 Published online by Cambridge University Press

(2.14) are transformed to

$$\tilde{S}'' - K_1 P^* \tilde{P} \mathrm{e}^{\tilde{S}} = 0, \tag{B 2a}$$

$$D_1 \tilde{S}_m'' + z_1 S_m'(z_1) - K_0 S_m(z_1) = 0, \tag{B 2b}$$

$$D_2 \tilde{P}'' - K_1 \tilde{P} \mathrm{e}^{\tilde{S}} = 0, \tag{B 2c}$$

$$D_3 \tilde{P}_m'' + K_1 \tilde{P} \mathrm{e}^{\tilde{S}} = 0, \tag{B 2d}$$

with errors of order $M^{-1} \log^2 M$. We denote the solutions in each of the three outer regions by using the appropriate subscript. The matching conditions are

$$\left.\begin{array}{l} \tilde{S}' \to S_1'(z_1) \\ \tilde{P}' \to P_1'(z_1) \\ \tilde{P}_m' \to P_{m1}'(z_1) \end{array}\right\} \text{ as } \zeta \to -\infty, \qquad \left.\begin{array}{l} \tilde{S}' \to S_2'(z_1) \\ \tilde{P} \to 0 \\ \tilde{P}_m' \to P_{m2}'(z_1) \end{array}\right\} \text{ as } \zeta \to +\infty. \tag{B 3}$$

Hence, we find that

$$\tilde{S}' - P^* D_2 \tilde{P}' = \text{constant} \qquad \text{and} \qquad D_2 \tilde{P}' + D_3 \tilde{P}_m' = \text{constant}, \tag{B 4}$$

which lead to the flux conditions (4.7d,e). A further integration yields

$$\tilde{S} = P^* D_2 \tilde{P} + S_2'(z_1)\zeta, \tag{B 5}$$

where the additional integration constant may be set to zero without loss of generality by exploiting the translation invariance in ζ. The resulting problem may be normalized by defining

$$\zeta = \frac{1}{S_2'(z_1)} \left[\log \left(\frac{D_2 s_2'(z_1)^2}{K_1} \right) + \xi \right], \qquad \tilde{P}(\zeta) = \frac{1}{P^* D_2} f(\xi), \tag{B 6}$$

so that $f(\xi)$ satisfies the ODE

$$\frac{\mathrm{d}^2 f}{\mathrm{d}\xi^2} = f \mathrm{e}^{f+\xi}, \tag{B 7}$$

subject to

$$\frac{\mathrm{d}f}{\mathrm{d}\xi} \to -\lambda \text{ as } \xi \to -\infty, \qquad f(\xi) \to 0 \text{ as } \xi \to +\infty, \tag{B 8}$$

where $\lambda = 1 - s_1'(z_1)/s_2'(z_1) \in (0, 1)$. There is a one-parameter family of solutions of (B 7) with permissible far-field behaviour of the form

$$f(\xi) \sim c \mathrm{K}_0 \left(2\mathrm{e}^{\xi/2} \right) \text{ as } \xi \to \infty, \tag{B 9}$$

where K_0 denotes a modified Bessel function and c is an arbitrary constant which may be used to shoot for a particular value of the slope λ at $-\infty$. Typical solutions are shown in Figure B 1 with different values of λ between 0 and 1.

https://doi.org/10.1017/S0956792515000327 Published online by Cambridge University Press

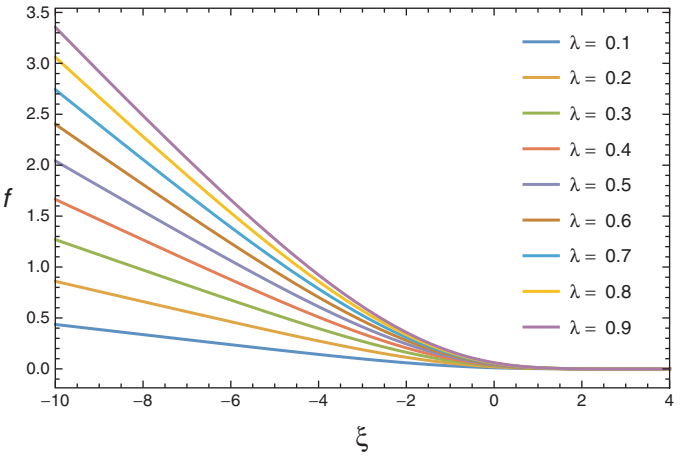

FIGURE B 1. The function $f(\xi)$ satisfying the ODE (B 7) and far-field conditions (B 8) with various values of $\lambda \in (0, 1)$.For interpretation of the references to colour in this figure, the reader is referred to the online version of this article.

To analyse the boundary layer at $z = z_3$, we perform the rescalings

$$z = z_2 + N^{-1/2}\eta, \qquad S_m(z) = S_m(z_3) + N^{-1/2}\eta S_m'(z_3) + N^{-1}\bar{S}_m(\eta), \tag{B 10a}$$

$$S(z) = 1 + N^{-1}\bar{S}(\eta), \qquad P_m(z) = P_m(z_3) + N^{-1/2}\eta P_m'(z_3) + N^{-1}\bar{P}_m(\eta). \tag{B 10b}$$

We recall that $P(z)$ is exponentially small here and hence is neglected. The resulting leading-order equations read

$$\bar{S}'' = K_0\left(\mathrm{e}^{\bar{S}} - S_m(z_3)\right), \tag{B 11a}$$

$$D_1\bar{S}_m'' = -z_3 S_m'(z_3) - K_0\left(\mathrm{e}^{\bar{S}} - S_m(z_3)\right), \tag{B 11b}$$

$$D_3\bar{P}_m'' = -z_3 P_m'(z_3). \tag{B 11c}$$

These are consistent with our assertion that S_m and P_m are continuously differentiable at $z = z_3$. We infer from (B 11c) that P_m'' is also continuous, which is to be expected since the leading-order solutions for P_m in regions 2 and 3 are identical. However, equation (B 11b) implies that S_m suffers a jump in its second derivative across $z = z_3$; again this is consistent with the solutions obtained in regions 2 and 3. It just remains to solve for $\bar{S}(\eta)$. The governing ODE (B 11a) may be normalized by the rescaling:

$$\eta = \frac{\xi}{\sqrt{K_0 S_m(z_3)}}, \qquad \bar{S}(\eta) = \log\big(S_m(z_3)\big) + g(\xi). \tag{B 12}$$

This results in

$$\frac{\mathrm{d}^2 g}{\mathrm{d}\xi^2} = \mathrm{e}^g - 1, \tag{B 13}$$

https://doi.org/10.1017/S0956792515000327 Published online by Cambridge University Press

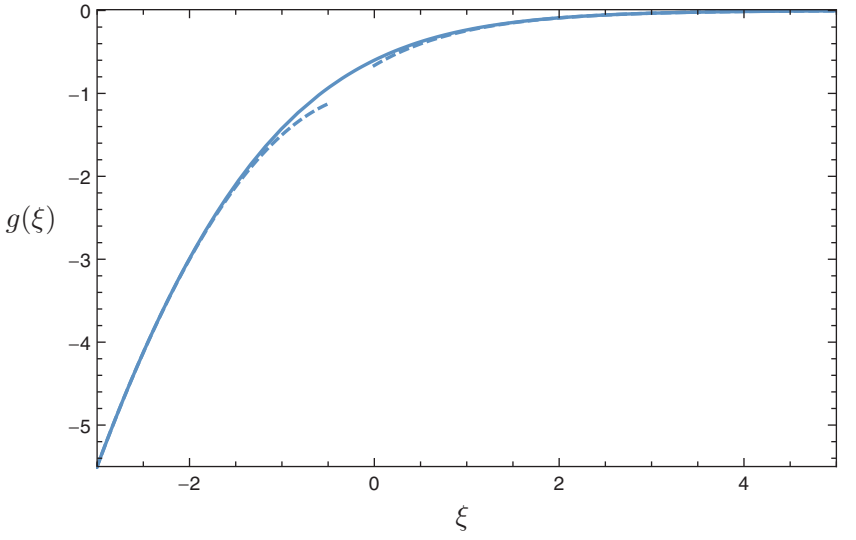

FIGURE B 2. The function $g(\xi)$ defined by equation (B 16). The dashed curves show the far-field asymptotic approximations (B 15) and (B 17)

which is to be solved subject to the far-field conditions

$$g(\xi) \sim -\frac{\xi^2}{2} \text{ as } \xi \to -\infty, \qquad g(\xi) \to 0 \text{ as } \xi \to -\infty. \tag{B 14}$$

These are consistent with the outer solution $S_3(z) \sim 1$ and with $S_2''(z_3) = -K_0 S_m(z_3)$, as implied by equation (4.8*a*). We choose to fix the arbitrary translation such that

$$g(\xi) \sim -\frac{\xi^2}{2} - 1 + o(1/\xi) \text{ as } \xi \to -\infty, \tag{B 15}$$

and the resulting solution takes the implicit form

$$\xi = -\sqrt{-2g} + \frac{1}{\sqrt{2}} \int_{-g}^{\infty} \left(\frac{1}{\sqrt{v + \mathrm{e}^{-v} - 1}} - \frac{1}{\sqrt{v}} \right) \mathrm{d}v. \tag{B 16}$$

The function $g(\xi)$ so defined is plotted in Figure B 2, along with the far-field behaviours (B 15) as $\xi \to -\infty$ and

$$g(\xi) \sim -C\mathrm{e}^{-\xi} \text{ as } \xi \to +\infty, \tag{B 17}$$

where

$$C = \exp\left[\frac{1}{\sqrt{2}} \int_1^{\infty} \left(\frac{1}{\sqrt{v + \mathrm{e}^{-v} - 1}} - \frac{1}{\sqrt{v}} \right) \mathrm{d}v \right.$$
$$\left. + \frac{1}{\sqrt{2}} \int_0^1 \left(\frac{1}{\sqrt{v + \mathrm{e}^{-v} - 1}} - \frac{1}{\sqrt{v}} - \frac{\sqrt{2}}{v} \right) \mathrm{d}v \right] \approx 0.66297. \tag{B 18}$$

https://doi.org/10.1017/S0956792515000327 Published online by Cambridge University Press

References

[1] Adamson, A. W. (1982) *Physical Chemistry of Surfaces*, Wiley, New York, USA.

[2] Bahramian, A. Thomas, R. K. & Penfold, J. (2014) The adsorption behavior of ionic surfactants and their mixtures with nonionic polymers and with polyelectrolytes of opposite charge at the air-water interface. *J. Phys. Chem. B* **118**(10), 2769–2783.

[3] Bain, C. D., Manning-Benson, S. & Darton, R. C. (2000) Rates of mass transfer and adsorption of hexadecyltrimethylammonium bromide at an expanding air-water interface. *J. Colloid Interface Sci.* **229**(1), 247–256.

[4] Bain, C. D. (2008) The overflowing cylinder sixty years on. *Adv. Colloid Interface Sci.* **144**(1), 4–12.

[5] Bell, C. G., Breward, C. J. W., Howell, P. D., Penfold, J. & Thomas, R. K. (2007) Macroscopic modelling of the surface tension of polymer–surfactant solutions. *Langmuir* **23**(11), 6042–6052.

[6] Bell, C. G., Breward, C. J. W, Howell, P. D., Penfold, J. & Thomas, R. K. (2010) A theoretical analysis of the surface tension profiles of strongly interacting polymer–surfactant systems. *J. Colloid Interface Sci.* **350**(2), 486–493.

[7] Breward, C. J. W., Darton, R. C., Howell, P. D. & Ockendon, J. R. (2001) The effect of surfactant on expanding free surfaces. *Chem. Eng. Sci.* **56**(8), 2867–2878.

[8] Breward, C. J. W., & Howell, P. D. (2004) Straining flow of micellar surfactant solution. *Eur. J. Appl. Math.* **15**(5), 511–531.

[9] Cabane, B. & Duplessix, R. (1985) Neutron-scattering study of water-soluble polymers adsorbed on surfactant micelles, *Colloid Surf.* **13**, 19–33.

[10] Goddard, E. D. (1986) Polymer–surfactant interaction part I. Uncharged water-soluble polymers and charged surfactants, *Colloid Surf.* **19**(2–3), 255–300.

[11] Goddard, E. D. (1986) Polymer–surfactant interaction part II. Polymer and surfactant of opposite charge. *Colloid Surf.* **19**(2–3), 301–329.

[12] Goddard, E. D. (2002) Polymer/surfactant interaction: Interfacial aspects. *J. Colloid Interface Sci.* **256**(1), 228–235.

[13] Goddard, E. D. & Ananthapadmanabhan, K. P. (1993) *Interactions of Surfactants with Polymers and Proteins*, CRC Press, Boca Raton.

[14] Howell, P. D. & Breward, C. J. W. (2002) Mathematical modelling of the overflowing cylinder experiment. *J. Fluid Mech.* **458**, 379–406.

[15] Kwak, J. C. T. (1998) *Polymer–Surfactant Systems*, Surfactant Science Series, Vol. 77, Marcel Dekker, New York.

[16] Monteux, C. (2014) Adsorption of soluble polymers at liquid interfaces and in foams. *C. R. Phys.* **15**(8), 775–785.

[17] Penfold, J., Sivia, D. S., Staples, E., Tucker, I., & Thomas, R. K. (2004) Surface ordering in dilute dihexadecyl dimethyl ammonium bromide solutions at the air–water interface. *Langmuir* **20**(6), 2265–2269.

[18] Purcell, I. P., Lu, J. R., Thomas, R. K., Howe, A. M. & Penfold, J. (1998) Adsorption of sodium dodecyl sulfate at the surface of aqueous solutions of poly(vinylpyrrolidone) studied by neutron reflection. *Langmuir* **14**(7), 1637–1645.